

Analytical approaches for wave energy dissipation induced by wave-generated turbulence and random wave-breaking

Yongzeng Yang ^{1,3}, Fuwei Wang ², Meng Sun ^{1,3}, Xingjie Jiang ^{1,3}, Xunqiang Yin ^{1,3},
Yongfang Shi ^{1,3}, and Yong Teng ¹

¹ First Institute of Oceanography, Ministry of Natural Resources, Qingdao, Shandong, China

² Frontier Science Center for Deep Ocean Multispheres and Earth System (FDOMES) and Physical Oceanography Laboratory, Ocean University of China, Qingdao, Shandong, China

³ Key Laboratory of Marine Science and Numerical Modeling (MASNUM), Ministry of Natural Resources, Qingdao, Shandong, China.

Correspondence: Meng Sun (sunm@fio.org.cn)

Abstract. This paper is dedicated to investigate the dissipation effects of wave-generated turbulence reacting on ocean waves and to estimate the energy loss due to wave-breaking theoretically. An analytical dissipation source function induced by wave-generated turbulence in the water was proposed through the equilibrium solutions of a second-order turbulence closure model between the wave shear instability generations and the turbulent kinetic energy (TKE) dissipations under the well-founded structural equilibrium closure assumptions. And an improved postbreaking spectrum expression, based on the breaking wave statistical method, was presented to depict more explicitly the intermittent wave-breaking events.

5 Comparisons of the TKE dissipation rates indicate that the model results agree well with the laboratory observations which were directly generated by the waves themselves, but for mechanical and wind waves, dispersions suggest the presence of other dynamic processes. The modeled attenuation coefficients of the breaking spectrum correspond to the decreasing tendency measured from the lake experiment,

10 which yields valuable insights of the physics of dominant breaking, but the statistical approach is less well-suited for simulating the rapid transient regime of wave breaking as well as for the higher frequency in the equilibrium range. Evaluations for more complex situations will be addressed in the future series of papers.

15

20 **1 Introduction**

The third generation ocean wave models, which integrate the dynamical equations that describe the evolution of a wave field, have been widely used in scientific studies and practical applications. Though input mechanisms, in particular bulk transfer of energy action and momentum to waves, and other source terms are not well
25 established either, the least understood aspect of the physics of wave model is the dissipation terms (Donelan and Yuan, 1994; Young and Babanin, 2006; Babanin, 2011). The dissipation source (sink) terms induced by wave-generated turbulence and random wave-breaking are the subject of the present paper. There are a number of dissipation mechanisms studied previously through either experimental or analytical
30 (or both) approaches, and they have advanced very significantly over the past decades. However, there remains a notable gap in mechanism research pertaining to varied parameterizations and applications in wave models.

Concerning to the wave-breaking dissipation, the most mathematically well-advanced and most frequently utilized whitecap model is that of Hasselmann (1974)
35 which involves the whitecaps are weak-in-the-mean and the dissipation is a linear function of the spectrum, and its parameterization has been proposed and further extended in various WAM-Cycle models by Komen et al. (1984), WAMDI G. (1988), Bidlot et al. (2005), Bidlot (2012), etc. Following the quasi-saturated ideas of Phillips (1985) and numerical modeling framework of Alves and Banner (2003), Ardhuin et al.
40 (2009, 2010), Filipot and Ardhuin (2012) presented an improved wave-breaking dissipation parameterization as the sum of the saturation-based term and a cumulative breaking term, while the latter represents the smoothing of the surface by big breakers that wipe out smaller waves. The probability model due to wave breaking was proposed by Longuet-Higgins (1969), Yuan et al (1986) and Hua and Yuan (1992).
45 This kind of wave-breaking dissipation source function was derived from the breaking wave statistics, in which the power of the normalized integral wave steepness parameter is $1/2$ and less than that of whitecap model. So the probability model gives lower dissipation value for the high sea state condition (Yuan et al., 1993), and has been applied in the LAGFD (Laboratory of Geophysical Fluid Dynamics)-WAM
50 wave model and MASNUM (Key Laboratory of MARine Science and NUMerical Modeling) wave model (Yuan et al., 1991; Yang et al., 2005). Though conceptually attractive, its practical parameterization fitted to the whitecap model is deprived of its

own discretionary estimates of the dissipation rate. Based on the random phase spectral action density balance equation for wavenumber-direction spectra and evolved from earlier WW1 and WW2 (WAVEWATCH I & II) model packages (Tolman, 1991, 1992), the comprehensive source terms were incorporated and employed in WW3 ((WAVEWATCH III) wave model by Tolman and Chalikov (1996), Chalikov and Belevich (1993), Chalikov (1995) , Tolman (2002), etc. Young and Babanin (2006) summarized series of previous experimental attempts to obtain an experimental spectral dissipation function, and based on direct estimates of wave energy loss due to dominant breaking through their comprehensive measurement records at Lake George, they proposed a new spectral dissipation source term due to wave breaking. This experimental parameterization was improved and employed in WW3 (WAVEWATCH III) wave model (Babanin et al., 2007, 2010; Babanin, 2009; Rogers et al., 2012; Liu et al., 2019; WW3DG, 2019). The quantitative match is dubious between the latter applications and the former experimental estimates, despite only a single field record was analyzed but verified approximately by turbulent kinetic energy (TKE) dissipation rates which were retrieved from synchronously ADV measured turbulence spectra (Young and Babanin, 2006). In addition, the physical meaning of wave-breaking dissipation rate (time derivative of wave energy spectrum), as stated in previous studies, remains fuzzy and vague because the wave-breaking process is not continuous but very short and intermittent, which stimulate us to propose an improved analytical postbreaking spectrum expression, from the point of view of the probability theory, for practical implementation. This constitutes one of our primary focal points of this study.

Polnikov (1994, 2005, 2010), Polnikov et al. (2006) argued that the mechanism of wave energy dissipation is completely conditioned by the interaction between wave motions and the turbulence of the upper water layer, and the latter is generated by a great number of physical processes, including different kinds of hydrodynamic instabilities of mechanical motions near the interface. They solved Reynolds' equation where the Reynolds' stress was expanded into a series with respect to velocity components and their spatial derivatives. The Prandtl mixing-length hypothesis was used to close the turbulent terms in these series. Their physical treatment is attractive, but the theory needs further development (Young and Babanin, 2006), even though it was further constructed by means of the phenomenological

similarity method and spectrally justified in the frame of the proposed eddy viscosity model (Polnikov, 2012). Tolman and Chalikov (1996) also suggested a turbulent dissipation analogy for tunable closure modeling. For dominant low-frequency dissipation, if wave motion and turbulence are not correlated, their interaction can be accounted for by introducing an effective, although weak, turbulent viscosity coefficient in the oceanic boundary layer. But for poorly understood high-frequency dissipation, a diagnostic high-frequency dissipation was defined and designed to result in a consistent source term balance. And the total dissipation source term was defined as a linear combination of the above high and low frequency constituents.

90 Their separation parameterization for the dissipation term is physically meaningful and the heuristic arguments have been employed in WW3 ST2 package and widely applied in many practical numerical models. In fact, during the past two decades, a series of studies concerned with mechanisms of nonbreaking wave-generated turbulence and its mixing effects on upper ocean layers have been achieved significantly and their conclusions have been confirmed more exhaustively by experiments. The theoretical wave-generated turbulence theory can be established by two different but relatively consistent approaches: the first approach involves the use of a parameterization form similar to the classical Prandtl mixing-length theory, and the second approach involves the use of the equilibrium solutions of a high-

100 deterministic second-order turbulence closure model between the wave motion shear instability generations and the TKE dissipations (Baumert et al., 2005), then the analytical mixing coefficients were proposed to elaborate the dominant mixing intensity induced by wave-generated turbulence in the upper ocean (Yuan et al., 1999; Yuan et al., 2013). Qualitative and quantitative validations by field measurements and improvements of wave-current coupled modelling indicate the key mixing role in the formation of upper mixed layers (Qiao et al., 2004, 2010; Xia et al., 2004, 2006; Shu et al., 2011; Shi et al., 2016, 2019; Yu et al., 2020; Zhuang et al., 2020, 2021, 2022; Yang et al., 2003, 2004, 2019, 2022). But how the reaction of wave-generated turbulence on ocean waves was disregarded in their studies, which is still lack and needs to investigate further. Babanin (2006), Babanin and Haus (2009), Dai et al.

105 (2010) tested and confirmed the nonbreaking wave-generated turbulence through mechanically generated laboratory wave experiments. Babanin and Chalikov (2012) also presented that the vorticity and turbulence usually occur in vicinity of wave crests and then spread over upwind slope and downward through a numerical wave-

115

120 turbulence model. Based on their experimental approximations, a parameterization of
swell dissipation rate was proposed, verified through altimeter observation data and
employed in WW3 ST6 package (Babanin 2011, 2012; Young et al., 2013; Zieger et
al., 2015; WW3DG, 2019). In fact, an analytical parameterization for wave energy
125 dissipation can be effectively deduced through the equilibrium solutions of wave-
generated turbulence, which will be described in detail and implemented in numerical
experiments below. It constitutes the other focal point of this study to illustrate the
important role of dissipation induced by wave-generated turbulence, which is
definitely the feedback of imparting of wave shear instability generations on
turbulence.

130 There are also a number of other dissipation mechanisms which are certainly not
negligible in the wave system. Prominent negative input source term for swell was
introduced by Chalikov & Belevich (1993), Chalikov (1995) , Tolman & Chalikov
(1996) , Tolman (2002) and Chalikov & Babanin (2009) where the phase velocity of
waves is larger than the wind velocity, which means that the dynamic pressure of the
135 wind on the forward face of the wave component exceeds the pressure on the
backward face and waves accelerate wind, resulting in the momentum and energy
fluxes from the waves to the wind. Based on the direct measurements of turbulent air-
sea fluxes obtained during several sea expeditions, Grachev and Fairall (2001)
verified that long ocean waves (swell) traveling faster than local wind and in the same
140 direction cause upward momentum transport, implying a negative drag coefficient. A
weak damping of swells was also introduced by Janssen (2004), who proposed an
asymptotic linearization of the small effects of air turbulent eddies. Ardhuin et al.
(2009, 2010) , Collard et al. (2009) proposed a nonlinear swell dissipation
parameterization, which is related to a laminar-to-turbulent transition of the
145 oscillatory boundary layer over swells, using the spaceborne SAR observed swell
fields from the European Space Agency's (ESA) ENVISAT satellite. Interaction of
ocean waves and upper ocean turbulence, while the latter is induced by Stokes drift
shears, accounts for a significant fraction of the energy losses of the wave field
(McWilliams et al., 1997; Teixeira and Belcher, 2002; Ardhuin and Jenkins, 2006;
150 Guo and Shen, 2013, 2014). Evaluations indicated it is much weaker than other
dissipations (Ardhuin et al., 2010), despite this its formula is employed in WW3 ST4
package. Model results showed that its effects significantly improve simulations of

turbulence characteristics and upper ocean thermal structure (Huang and Qiao, 2010; Huang et al., 2011). Sea bottom-wave interactions and ice-wave interactions have
155 been studied in great detail, which are out of scope of present study and not discussed here.

The objectives of this paper are to explore the dissipation effects of wave-generated turbulence reacting on ocean waves, and to investigate the role of wave-breaking dissipation via an improved postbreaking spectrum expression based on the
160 breaking wave statistical method. The remainder of this paper is organized as follows: Section 2 describes the analytical approaches for wave energy dissipation induced by wave-generated turbulence and by random wave-breaking, introduces scale detection comparing to wind input and provides verifications with laboratory observations or comprehensive measurements; Section 3 presents application implementations on
165 simple duration-limited growth and decay experiments; Section 4 addresses discussions and issues which need complex insights, and some conclusions and suggestions for future research are summarized in Section 5.

2 Model derivation and verification

2.1 The analytical approach for wave energy dissipation induced by wave-generated turbulence 170

In the usual notation, let $x_i, i = 1, 2, 3$ be rectangular co-ordinates (The list of symbols is provided in Appendix D). Let $u_{SMi}, i = 1, 2, 3$ denote the wave velocities;
 $T_{SM}, s_{SM}, p_{SM}, \rho_{SM}$ the perturbations of temperature, salinity, pressure and density induced by ocean waves. More comprehensive governing equations for wave motion
175 were derived in Yuan et al.(2012) and Yang et al. (2022) under the assumption that turbulence timescale is much shorter than wave period, and the unit volume wave energy balance equation can be obtained in tensor expression as follows (see Appendix A):

$$\begin{aligned}
& \frac{\partial}{\partial t} \left\langle \frac{\rho_0 u_{SMi}^2}{2} + \frac{g^2 \rho_{SM}^2}{2\rho_0 \hat{N}_3^2} \right\rangle_{SM} + \left\langle (\hat{U}_j + u_{SMj}) \frac{\partial}{\partial x_j} \left(\frac{\rho_0 u_{SMi}^2}{2} + \frac{g^2 \rho_{SM}^2}{2\rho_0 \hat{N}_3^2} \right) \right\rangle_{SM} + \frac{\partial}{\partial x_i} \langle p_{SM} u_{SMi} \rangle_{SM} \\
& = \left(-\rho_0 \langle u_{SMi} u_{SMj} \rangle_{SM} \frac{\partial \hat{U}_i}{\partial x_j} + g \langle \rho_{SM} u_{SM\alpha} \rangle_{SM} \frac{\hat{N}_\alpha^2}{\hat{N}_3^2} + \frac{g^2}{\rho_0 \hat{N}_3^2} \langle \rho_{SM} Q_{\rho SM} \rangle_{SM} \right. \\
& \left. + \left[\frac{\partial}{\partial x_j} \left\langle \left(v_0 + \frac{k^2}{\pi^2 \varepsilon} \right) \frac{\partial}{\partial x_j} \left(\frac{\rho_0 u_{SMi}^2}{2} \right) \right\rangle_{SM} + \frac{\partial}{\partial x_j} \left\langle \left(K_0 + \frac{1}{\sigma_0} \frac{k^2}{\pi^2 \varepsilon} \right) \frac{\partial}{\partial x_j} \left(\frac{g^2 \rho_{SM}^2}{2\rho_0 \hat{N}_3^2} \right) \right\rangle_{SM} \right] \right. \\
& \left. + \left[-\left\langle \rho_0 \left(v_0 + \frac{k^2}{\pi^2 \varepsilon} \right) \left(\frac{\partial u_{SMi}}{\partial x_j} \right)^2 \right\rangle_{SM} - \left\langle \frac{g^2}{\rho_0 \hat{N}_3^2} \left(K_0 + \frac{1}{\sigma_0} \frac{k^2}{\pi^2 \varepsilon} \right) \left(\frac{\partial \rho_{SM}}{\partial x_j} \right)^2 \right\rangle_{SM} \right] \right\}
\end{aligned}$$

180 (1)

where $\hat{U}_i, i=1,2,3; \hat{T}, \hat{s}, \hat{p}, \hat{\rho}$ denote the background current components and ρ_0 is the basin mean water density; v_0, K_0, D_0 the molecular viscosity, thermal and diffusion coefficients; $\hat{N}_i^2 = -g \frac{\partial}{\partial x_i} \left(\frac{\hat{\rho}}{\rho_0} \right), i=1,2,3$ the Brunt–Väisälä frequency components;

$\sigma_0 = \frac{1}{2}$ the Prandtl number; k, ε the kinetic energy and its dissipation rate of ocean

185 turbulence, which is generated by shear instability of background current (Mellor and Yamada, 1982), Stokes drift (Ardhuin and Jenkins, 2006; Ardhuin et al, 2010; Huang and Qiao, 2010) but mainly generated by ocean waves in the upper layers (Yuan et al., 1999, 2013; Qiao et al., 2004; Yang et al. , 2003, 2004; Babanin, 2006; Babanin and Haus, 2009; Dai et al., 2010; Zhuang et al., 2022). $\frac{\rho_0 u_{SMi}^2}{2}, \frac{g^2 \rho_{SM}^2}{2\rho_0 \hat{N}_3^2}$ denote the kinetic and

190 potential wave energy and $\langle \cdot \rangle_{SM}$ denotes the Reynolds average on the wave motion.

Hereafter, other symbols have their usual meaning. The first term on the left-hand side of Eq. (1) is related to the local mechanical energy variation and the second and third ones denote the energy flux transferred by ocean waves and background currents. The first and second terms on the right-hand side of Eq. (1) are related to the modulation by larger scale motions through shear instability generations. The third term is related to the energy input through thermal radiation, the fourth and fifth ones are related to the modulation by smaller scale motions through ocean mixing and the last two terms are related to the energy loss rate due to internal viscosity. It should be noted that three types of gravity ocean waves, which consist of surface waves, internal waves and inertial waves, follow the same governing Eq. (1). Here in this study only the former is concerned, so the fifth term on the right-hand side of Eq. (1) is the energy dissipation induced by ocean turbulence (Dissipation induced by molecular viscosity is insignificant and not considered here).

200

As stated above, ocean wave-generated turbulence plays a dominant role in the
 205 upper layers, the energy loss from ocean waves needs to be studied further. The unit
 volume energy dissipation mainly induced by wave-generated turbulence can be
 expressed as

$$-\left\langle \rho_0 \frac{k^2}{\pi^2 \varepsilon} \left(\frac{\partial u_{SMi}}{\partial x_j} \right)^2 \right\rangle_{SM} = -\rho_0 \alpha_{wt} \left\langle \frac{\bar{k}^2}{\pi^2 \bar{\varepsilon}} \right\rangle_{SM} \left\langle \left(\frac{\partial u_{SMi}}{\partial x_j} \right)^2 \right\rangle_{SM} \quad (2)$$

210 where the symbol overbar ‘-’ denotes the turbulent equilibrium variables, $\left\langle \frac{\bar{k}^2}{\pi^2 \bar{\varepsilon}} \right\rangle_{SM}$ is
 the so-called wave-generated turbulent mixing coefficient which was widely used in
 coupling numerical models. α_{wt} is an undetermined constant here, which implies the
 quasi-equilibrium level of wave-generated turbulence. Then the total energy
 dissipation for vertical water column per unit area can be written as

$$215 \quad -\int_{-\hat{H}}^0 \left\langle \rho_0 \frac{k^2}{\pi^2 \varepsilon} \left(\frac{\partial u_{SMi}}{\partial x_j} \right)^2 \right\rangle_{SM} dx_3 = -\rho_0 \alpha_{wt} \int_{-\hat{H}}^0 \left\langle \frac{\bar{k}^2}{\pi^2 \bar{\varepsilon}} \right\rangle_{SM} \left\langle \left(\frac{\partial u_{SMi}}{\partial x_j} \right)^2 \right\rangle_{SM} dx_3 \quad (3)$$

where \hat{H} denotes the water depth.

In the statistical wave theory, the wave field is regarded as weakly-in-the-mean
 nonlinear processes and the chief linear components are used widely for further
 220 detection (Komen et al., 1994). Below we try to derive the total energy dissipation
 expressed by wavenumber spectrum through the classical linear wave solutions, i.e.,

$$u_{SM1} = \iint_{\bar{k}} \frac{\omega k_1}{K} A \frac{\cosh K(\hat{H} + x_3)}{\sinh K\hat{H}} \exp\{i(\bar{\mathbf{k}} \cdot \bar{\mathbf{r}} - \omega t)\} d\bar{\mathbf{k}} \quad (4)$$

$$225 \quad u_{SM2} = \iint_{\bar{k}} \frac{\omega k_2}{K} A \frac{\cosh K(\hat{H} + x_3)}{\sinh K\hat{H}} \exp\{i(\bar{\mathbf{k}} \cdot \bar{\mathbf{r}} - \omega t)\} d\bar{\mathbf{k}} \quad (5)$$

$$u_{SM3} = \iint_{\bar{k}} -\omega i A \frac{\sinh K(\hat{H} + x_3)}{\sinh K\hat{H}} \exp\{i(\bar{\mathbf{k}} \cdot \bar{\mathbf{r}} - \omega t)\} d\bar{\mathbf{k}} \quad (6)$$

where the wavenumber vector $\bar{\mathbf{k}} = (k_1, k_2)$ with $K = \sqrt{k_1^2 + k_2^2}$, $\bar{\mathbf{r}} = (x_1, x_2)$. ω

denotes the radian frequency, and A , the wave amplitude.

230 For a spatially homogeneous and temporally stationary wave field, the product

$$\left\langle \frac{\partial u_{SMi}}{\partial x_1} \frac{\partial u_{SMi}}{\partial x_1} \right\rangle_{SM} \text{ is simplified as}$$

$$\begin{aligned} \left\langle \frac{\partial u_{SMi}}{\partial x_1} \frac{\partial u_{SMi}}{\partial x_1} \right\rangle_{SM} &= \iint_{\bar{k}} \text{Re} \left\{ \iint_{\bar{k}'} \omega \omega' \frac{k_1^2}{K} \frac{k_1'^2}{K'} \frac{\cosh K(\hat{H} + x_3)}{\sinh K\hat{H}} \frac{\cosh K'(\hat{H} + x_3)}{\sinh K'\hat{H}} \right. \\ &\quad \left. \left\langle AA^* \exp \left\{ i \left[(k_\alpha - k'_\alpha)x_\alpha - (\omega - \omega')t \right] \right\} \right\rangle dk_1 dk_2' \right\} dk_1 dk_2 \\ &= \iint_{\bar{k}} \text{Re} \left\{ \iint_{\bar{k}'} \omega \omega' \frac{k_1^2}{K} \frac{k_1'^2}{K'} \frac{\cosh K(\hat{H} + x_3)}{\sinh K\hat{H}} \frac{\cosh K'(\hat{H} + x_3)}{\sinh K'\hat{H}} \right. \\ &\quad \left. \delta(\bar{k} - \bar{k}') E(k_1, k_2) dk_1 dk_2' \right\} dk_1 dk_2 \\ &= \iint_{\bar{k}} \omega^2 \frac{k_1^4}{K^2} \frac{\cosh^2 K(\hat{H} + x_3)}{\sinh^2 K\hat{H}} E(k_1, k_2) dk_1 dk_2 \end{aligned}$$

(7)

where $\delta(\cdot)$ denotes the Dirac function and $E(k_1, k_2)$, the wavenumber spectrum

235 (Kinsman, 2012).

Correspondingly, after some similar manipulations and summing over all product terms, we obtain

$$\left\langle \frac{\partial u_{SMi}}{\partial x_j} \frac{\partial u_{SMi}}{\partial x_j} \right\rangle_{SM} = \iint_{\bar{k}} 2\omega^2 K^2 \frac{\cosh 2K(\hat{H} + x_3)}{\sinh^2 K\hat{H}} E(k_1, k_2) dk_1 dk_2$$

(8)

240 Hence,

$$\begin{aligned} - \int_{-\hat{H}}^0 \left\langle \rho_0 \frac{k^2}{\pi^2 \varepsilon} \left(\frac{\partial u_{SMi}}{\partial x_j} \right)^2 \right\rangle_{SM} dx_3 &= -\rho_0 g \iint_{\bar{k}} 2\alpha_{wt} \frac{\omega^2 K^2}{g} \left[\int_{-\hat{H}}^0 \left\langle \frac{\bar{k}^2}{\pi^2 \varepsilon} \right\rangle_{SM} \frac{\cosh 2K(\hat{H} + x_3)}{\sinh^2 K\hat{H}} dx_3 \right] E(k_1, k_2) dk_1 dk_2 \\ &= -\rho_0 g \iint_{\bar{k}} 2\alpha_{wt} \frac{\omega^2 K^2}{g} \left\{ \frac{\iint_{\bar{k}} \omega^2 K^2 \left[\int_{-\hat{H}}^0 \left\langle \frac{\bar{k}^2}{\pi^2 \varepsilon} \right\rangle_{SM} \frac{\cosh 2K(\hat{H} + x_3)}{\sinh^2 K\hat{H}} dx_3 \right] E(k_1, k_2) dk_1 dk_2}{\iint_{\bar{k}} \omega^2 K^2 E(k_1, k_2) dk_1 dk_2} \right\} E(k_1, k_2) dk_1 dk_2 \end{aligned}$$

(9)

The dissipation source function induced by wave-generated turbulence can be expressed in wavenumber space as

$$245 \quad S_{\text{tid}} = -2\alpha_{\text{wt}} \frac{\omega^2 K^2}{g} \left\{ \frac{\iint_{\vec{k}} \omega^2 K^2 \left[\int_{-\hat{H}}^0 \left\langle \frac{\bar{k}^2}{\pi^2 \bar{\varepsilon}} \right\rangle_{\text{SM}} \frac{\cosh 2K(\hat{H} + x_3)}{\sinh^2 K\hat{H}} dx_3 \right] E(k_1, k_2) dk_1 dk_2}{\iint_{\vec{k}} \omega^2 K^2 E(k_1, k_2) dk_1 dk_2} \right\} E(k_1, k_2)$$

(10)

For deep water depth, it is easily derived as

$$S_{\text{tid}} = -4\alpha_{\text{wt}} K^3 \left\{ \frac{\iint_{\vec{k}} \omega^2 K^2 \left[\int_{-\infty}^0 \left\langle \frac{\bar{k}^2}{\pi^2 \bar{\varepsilon}} \right\rangle_{\text{SM}} \exp\{2Kx_3\} dx_3 \right] E(k_1, k_2) dk_1 dk_2}{\iint_{\vec{k}} \omega^2 K^2 E(k_1, k_2) dk_1 dk_2} \right\} E(k_1, k_2)$$

(11)

250 Yuan et al. (2013) proposed a parameterization of the mixing coefficient $\left\langle \frac{\bar{k}^2}{\pi^2 \bar{\varepsilon}} \right\rangle_{\text{SM}}$

through equilibrium solutions of the second-order turbulence model under the well-founded structural equilibrium closure assumptions, in which the power function relationship between turbulent dissipation rate and shear instability generation of wave motion was fitted by observation data in deep ocean. Here we choose a generic

255 representation of the mixing length of $\bar{l}_D = \frac{\bar{k}^{-3/2}}{\pi^{3/2} \bar{\varepsilon}}$ (Baumert et al., 2005), which is

appropriate for deep and shallow water conditions, and the mixing coefficient is formulated conveniently as (The derivation processes to the following Eq. (12) and Eqs. (15, 19) are provided in Appendix B)

$$260 \quad \left\langle \frac{\bar{k}^2}{\pi^2 \bar{\varepsilon}} \right\rangle_{\text{SM}} = \frac{\sqrt{7}}{2} \iint_{\vec{k}} E(k_1, k_2) \frac{\cosh^2 K(\hat{H} + x_3)}{\sinh^2 K\hat{H}} dk_1 dk_2 \left(\iint_{\vec{k}} \omega^2 K^2 \frac{\cosh 2K(\hat{H} + x_3)}{\sinh^2 K\hat{H}} E(k_1, k_2) dk_1 dk_2 \right)^{1/2}$$

(12)

For deep water depth, Eq. (12) is reduced to

$$\left\langle \frac{\bar{k}^2}{\pi^2 \bar{\varepsilon}} \right\rangle_{\text{SM}} = \sqrt{\frac{7}{2}} \iint_{\vec{k}} E(k_1, k_2) \exp\{2Kx_3\} dk_1 dk_2 \left(\iint_{\vec{k}} \omega^2 K^2 E(k_1, k_2) \exp\{2Kx_3\} dk_1 dk_2 \right)^{1/2}$$

(13)

Now we try to present a concise description of Eq. (11) for future practical
265 application, some characteristic wavenumbers and frequencies are introduced for various integral mean variables, i.e.,

$$\iint_{\vec{k}} E(k_1, k_2) \exp\{2Kx_3\} dk_1 dk_2 \approx \exp\{2\hat{K}_1 x_3\} \iint_{\vec{k}} E(k_1, k_2) dk_1 dk_2, \quad \iint_{\vec{k}} \omega^2 K^2 E(k_1, k_2) \exp\{2Kx_3\} dk_1 dk_2 \approx \hat{\omega}^2 \hat{K}_2^2 \exp\{2\hat{K}_2 x_3\} \iint_{\vec{k}} E(k_1, k_2) dk_1 dk_2 \quad \text{and}$$

$\iint_{\hat{k}} \frac{1}{2K + 2\hat{K}_1 + \hat{K}_2} \omega^2 K^2 E(k_1, k_2) dk_1 dk_2 \approx \frac{1}{5K^3} \iint_{\hat{k}} \omega^2 K^2 E(k_1, k_2) dk_1 dk_2$, here we assume that $\hat{K}_1 \approx \hat{K}_2 \approx \hat{K}_3 \approx \hat{K}$

approximately. Then Eq. (13) is reduced to

$$270 \quad \left\langle \frac{\bar{k}^2}{\pi^2 \bar{\varepsilon}} \right\rangle_{SM} \approx \sqrt{\frac{7}{2}} \hat{\omega} \hat{K} \left(\iint_{\hat{k}} E(k_1, k_2) dk_1 dk_2 \right)^{\frac{3}{2}} \exp\{3\hat{K}x_3\}$$

(14)

By employing Eq. (14), Eq. (11) is derived approximately as

$$S_{tid} \approx -\frac{2\sqrt{14}}{5} \alpha_{wt} K^3 \hat{\omega} \left(\iint_{\hat{k}} E(k_1, k_2) dk_1 dk_2 \right)^{\frac{3}{2}} E(k_1, k_2)$$

(15)

275 For finite water depth, a simple scaling factor $R_H = 1 - \exp(-5KH)$ is introduced to Eq. (15) for numerical implementation.

We further detect the scales of the dissipation rate comparing to the wind input source function. There are still a relative large uncertainties remained in different bulk energy input approaches, here only the parameterizations of growth rate due to wind, which were proposed by Komen et al. (1984) and Janssen (1991), are concerned for the following convenient arguments. The growth rate of the wave scales with wavenumber was thought of as $\gamma \sim k^{3/2}$ (Janssen 1991), for

$$\gamma \sim \beta \frac{\omega}{C^2} u_*^2 = g^{-1/2} \beta K^{3/2} u_*^2, \text{ where } u_* \text{ is the friction velocity, } c \text{ the phase velocity}$$

285 $c = \frac{\omega}{K}$, β the Miles parameter $\beta = \frac{1.2}{K^2} \mu \ln^4 \mu$, $\mu \leq 1$ and μ the dimensionless critical height. Moreover, it can also be rewritten as

$$\gamma \sim \beta \frac{\omega}{C^2} u_*^2 = K \beta \left(\frac{u_*}{C} \right) u_* = K \beta \alpha^{-1/2} (Kz_0)^{1/2} u_* = K \tilde{l}_j u_*, \quad \tilde{l}_j = \alpha^{-1/2} \beta (Kz_0)^{1/2}$$

(16)

where z_0 is the sea surface roughness, and α , the Charnock constant. The dimensionless variable $\tilde{l}_j \sim \beta (Kz_0)^{1/2}$ is related to the dimensionless critical height μ and the relative roughness length Kz_0 . Incidentally, the growth rate parameterized by Komen et al. (1984) is fairly linearized as follows:

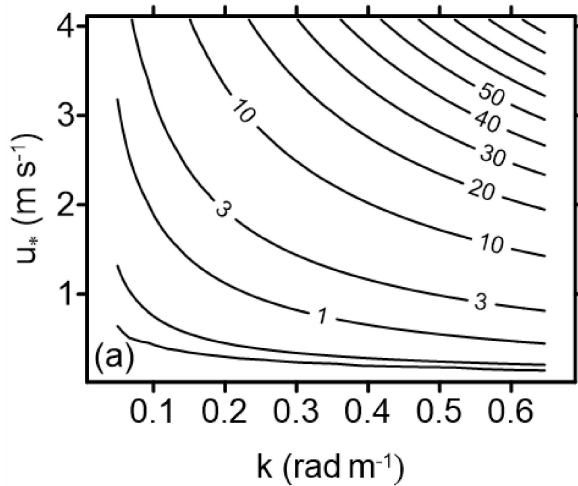
290

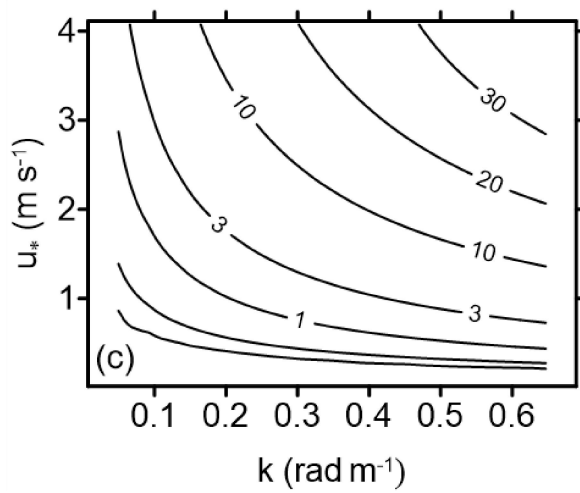
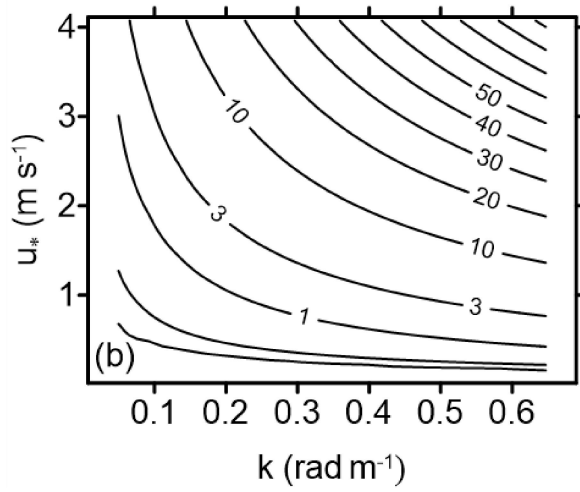
$$\gamma' \sim \frac{\omega}{C} u_* = K u_*.$$

From Eq. (15), the dissipation rate induced by wave-generated turbulence can be rescaled as

$$\begin{aligned} \gamma_{\text{tid}} &\sim \frac{2\sqrt{14}}{5} \alpha_{\text{wt}} K^3 \hat{\omega} \frac{A^3}{2^{3/2}} \\ 295 \quad &= \frac{\sqrt{7}}{5} \alpha_{\text{wt}} K^3 A^2 (A\hat{\omega}) = \frac{\sqrt{7}}{5} \alpha_{\text{wt}} K (KA)^2 u_{w0} = K \tilde{l}_Y u_{w0}, \quad \tilde{l}_Y = \frac{\sqrt{7}}{5} \alpha_{\text{wt}} (KA)^2 \end{aligned} \quad (17)$$

where u_{w0} is the wave orbital velocity at sea surface. $\tilde{l}_Y \sim (KA)^2$ can be taken to be some kind of dimensionless height or wave steepness. Hence Eq. (16) and (17) yield a considerable uniformity of analytical expressions. Figure 1 shows the growth rate γ roughly calculated under the condition $\frac{\tau_w}{\tau} = 0.2, 0.5, 0.9$ respectively, where τ_w is the wave-induced stress and $\tau = u_*^2$ the total stress, and the final subplot corresponds to the severe sea state scenario. Figure 2 shows the dissipation rate γ_{tid} with $\alpha_{\text{wt}} = 1.0$ in consideration of the breaking criterion that u_{w0} does not exceed the phase velocity of waves. Both are comparable in spatial distribution and magnitude, especially under normal and extreme sea conditions. And the corresponding spectral signatures of difference between Fig. 1 and 2 dominate the wave growth or decay.





310 **Figure 1.** Distribution of growth rate γ as a function of wavenumber and friction velocity (Unit: s^{-1}). **(a)** $\frac{\tau_w}{\tau} = 0.2$; **(b)** $\frac{\tau_w}{\tau} = 0.5$; **(c)** $\frac{\tau_w}{\tau} = 0.9$.

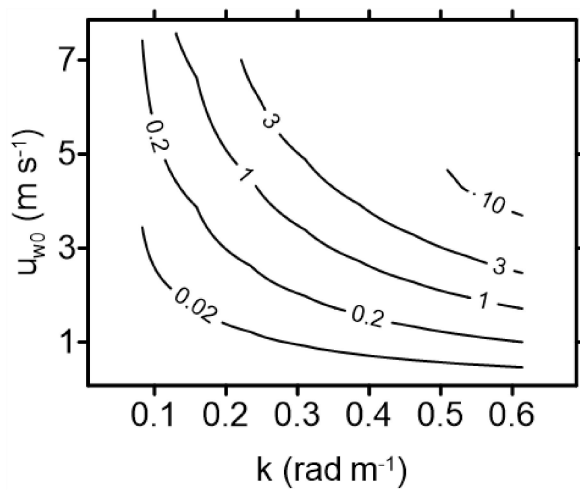


Figure 2. Distribution of dissipation rate γ_{tid} as a function of wavenumber and wave orbital velocity at sea surface (Unit: s^{-1})

315 The unit volume wave energy dissipation rate induced by wave-generated

turbulence is $e_{\text{tid}} = \left\langle \frac{k^2}{\pi^2 \bar{\varepsilon}} \left(\frac{\partial u_{\text{SM}i}}{\partial x_j} \right)^2 \right\rangle_{\text{SM}} = \alpha_{\text{wt}} \left\langle \frac{\bar{k}^2}{\pi^2 \bar{\varepsilon}} \right\rangle_{\text{SM}} \left\langle \left(\frac{\partial u_{\text{SM}i}}{\partial x_j} \right)^2 \right\rangle_{\text{SM}}$ following from Eq. (2), and

according the equilibrium solutions of the generation term to the dissipation for wave-generated turbulence (Yuan et al., 2013), the TKE dissipation rate ε_{dis} can be virtually identical to e_{tid} , i. e.,

$$320 \quad \varepsilon_{\text{dis}} \approx e_{\text{tid}} = \alpha_{\text{wt}} \left\langle \frac{\bar{k}^2}{\pi^2 \bar{\varepsilon}} \right\rangle_{\text{SM}} \left\langle \left(\frac{\partial u_{\text{SM}i}}{\partial x_j} \right)^2 \right\rangle_{\text{SM}} \quad (18)$$

There are many studies to verify the modeled TKE dissipation rate ε_{dis} , generated by shear instability of irregular wind waves or swells, with cruise observations (Yuan et al., 2013; Zhuang et al., 2020, 2021). Here a direct comparison between modeled

325 ε_{dis} with laboratory observations is performed for monochromatic non-breaking waves. In consideration of an approximate coefficient 7/8 introduced from the minimization relation for the equilibrium solutions (Yuan et al., 2013), the TKE dissipation rate ε_{dis} can be derived as

$$330 \quad \varepsilon_{\text{dis}} \approx \alpha_{\text{wt}} \frac{7}{8} \left\langle \frac{\bar{k}^2}{\pi^2 \bar{\varepsilon}} \right\rangle_{\text{SM}} \left\langle \left(\frac{\partial u_{\text{SM}i}}{\partial x_j} \right)^2 \right\rangle_{\text{SM}} = \frac{7\sqrt{7}}{16} \alpha_{\text{wt}} A^5 \omega^3 K^3 \exp\{5K\chi\} \quad (19)$$

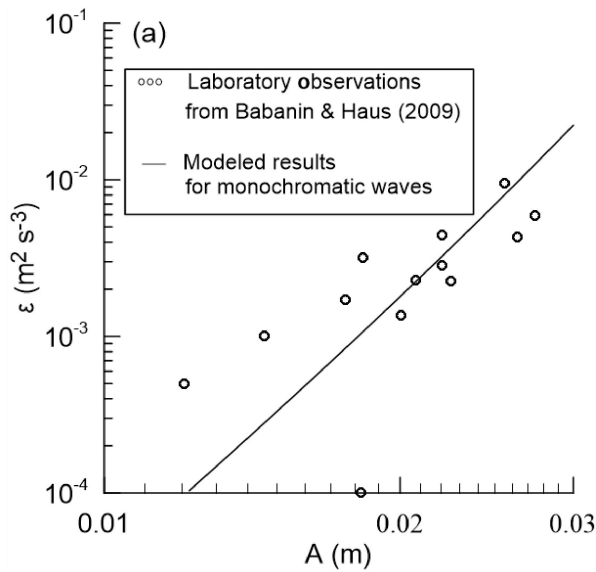
where A is the monochromatic wave amplitude at surface.

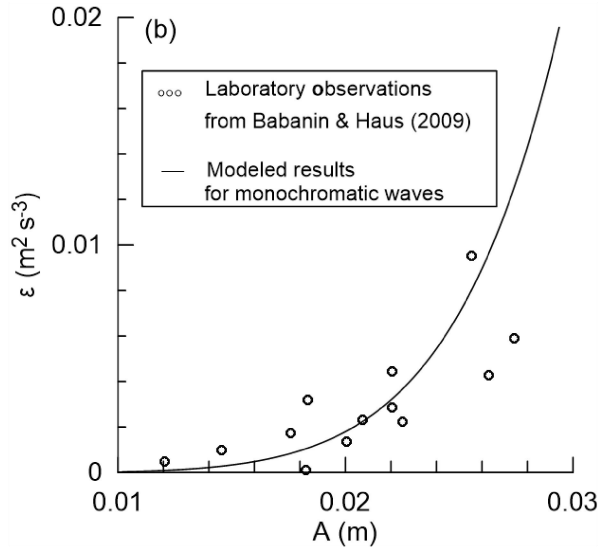
Two sets of experimental data are selected to verify the modeled TKE dissipation rate ε_{dis} below. For the first set of laboratory measurements, in order to avoid ambiguity due to wind-caused shear stresses and other dynamic mechanisms, a simple

335 setup for unforced mechanically generated monochromatic wave trains was realized. For the second set of laboratory measurements, wave-induced turbulence with regard to the wind wave, swell and mixed wave conditions, as well as the decreasing tendency of the TKE dissipation rate with layer depth, was conducted for joint comparisons.

340 The ‘‘observed’’ TKE dissipation rates ε_{dis} in the first set of experimental data come from the laboratory measurements conducted in the Air-Sea Interaction Saltwater Tank (ASIST) of the University of Miami (Babanin and Haus, 2009;

Babanin, 2011), with generated wave trains of $f=1.5$ Hz and $K_{1.5\text{Hz}}= 9.82$ rad m^{-1} . The significant TKE dissipation rates ε_{dis} were retrieved from the wavenumber spectra provided by Particle Image Velocimetry (PIV) measurements at the 30 mm layer from the still surface. Their detailed experimental measurements indicate that the turbulence observed must have been directly generated by the waves themselves (Babanin and Haus, 2009). Figure 3 shows the dependence of TKE dissipation rate ε_{dis} versus wave amplitude A in logarithmic and linear scales respectively, and the solid line is plotted by using Eq. (19) with $\alpha_{\text{wt}} = 1.0$ (Layer depth x_3 varies corresponding to different A). Babanin (2011) interpreted that the “observed” ε_{dis} are instantaneous values incurred intermittently at the rear-face phase of the wave below the level of the wave trough, and if averaged over the wave period, the estimates of ε_{dis} have to be divided at least by a factor of 10 and perhaps more. This implies that such intermittent turbulence is still at the stage of quasi-equilibrium level, and the coefficient $\alpha_{\text{wt}} = 1.0$ should be tuned to less than one order of magnitude or more for practical application (Wang et al., 2024).





360 **Figure 3.** Dependence of TKE dissipation rate ε_{dis} (denoted as ε in the figure) versus wave amplitude A . Observation data (circles) are digitalized from Babanin and Haus (2009). Dependence (19) is shown with a solid line. Data are plotted in **(a)** logarithmic scales and **(b)** linear scales.

In the second set of experimental data, the ‘‘observed’’ TKE dissipation rates ε_{dis} with different layer depth come from the laboratory measurements performed inside a wave tank at the Institute of Applied Physics of the Russian Academy of Science, Nizhny Novgorod, Russia (Wei et al., 2018). The tank was equipped with a mechanical wavemaker and a fan, which are used to generate mechanical and wind waves respectively. The vertical surface displacement of the generated wind waves and swell trains were measured by 3 resistancetype wave gages, and series of larger waves are selected for our further comparisons (Table 1).

Experiment number	Wave condition	H_s (cm)	Peak frequency (Hz)	Wave length (m)
1	21 m s ⁻¹ wind	3.75	2.72	0.42
2	32 m s ⁻¹ wind	6.03	1.97	0.83
3	1.6 Hz swell with 21 m s ⁻¹ wind	5.26	1.64	0.86
4	1.2 Hz swell	3.98	1.20	1.36

Table 1. Significant wave height (H_s) and peak frequency for selected wave conditions from Wei et al. (2018)

The TKE dissipation rates ε_{dis} at different layers from surface were retrieved from the wavenumber spectra provided by underwater 3-D instantaneous velocity measured by using an Acoustic Doppler Velocimeter (SonTek microADV). As Thais and Magnaudet (1996) interpreted their experimental observations, the wave orbital motions, which possess strong vertical gradients, ought to be the dominate role of enhancing of the turbulence production. Figure 4 shows the dependence of TKE dissipation rate ε_{dis} versus layer depth in linear/logarithmic scale for various wave conditions respectively, and the solid lines are plotted also by using Eq. (19) with $\alpha_{\text{wt}} = 1.0$ (A is the mean amplitude of the highest one-third or one-half waves). The decreasing tendency of modeled ε_{dis} with layer depth under different wave conditions agrees with that of observations in the upper 0.2 m layers. It should be noted that when the layer depth is larger than 0.25 m, the “observed” ε_{dis} may be regarded as adaptive noises induced by other dynamic mechanisms.

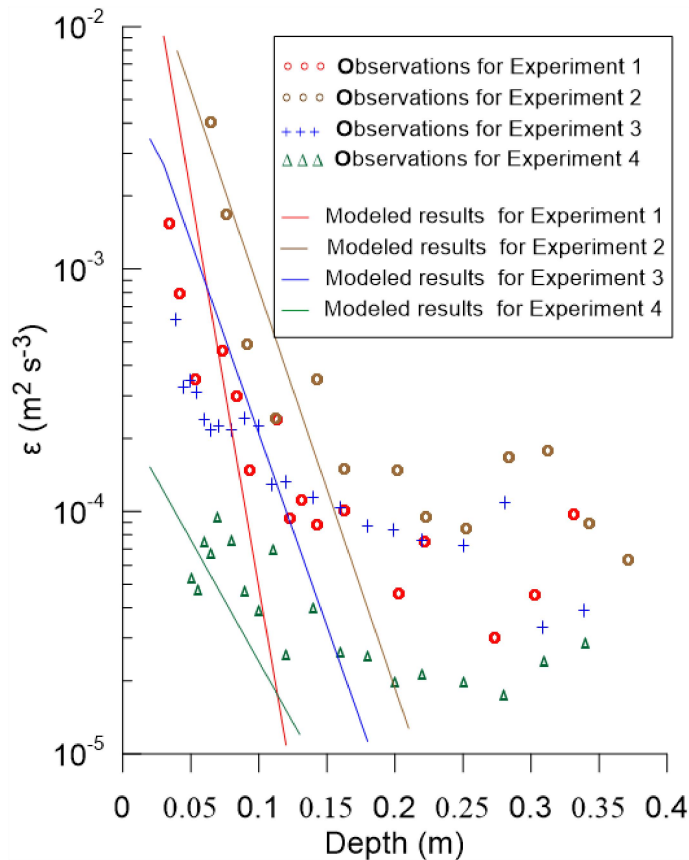


Figure 4. Dependence of TKE dissipation rate ε_{dis} (denoted as ε in the figure) versus layer depth. Observation data (circles, pluses and triangles) are digitalized from Wei et al. (2018). Dependence (19) is shown with solid lines. Data are plotted in linear/logarithmic scale on the horizontal/vertical axis.

The turbulence production is attributed to the wave-generation conditions. The turbulence observed in the first set of measurement data is directly generated by the waves themselves. While in the second set of measurement data, turbulence generation may be governed by complex dynamical mechanisms, including wave breaking, wind-driven turbulence, Langmuir turbulence, etc., and only the shear instability of wave orbital motions to turbulence is considered here. Preliminary studies indicate that the latter may be the dominant contributor to turbulence, their detailed comparisons are provided in Supplementary material (S1). The “observed” TKE dissipation rates ε_{dis} in both sets of measurement data correspond to the instantaneous state when turbulence occurs, and in the above comparative experiments we set the quasi-equilibrium coefficient $\alpha_{\text{wt}} = 1.0$ in our model for the estimates of ε_{dis} . This introduces uncertainty with regard to phase averaging in practical numerical modeling, which is discussed further in Section 4.

405

2.2 The precise estimation of wave energy loss induced by random wave-breaking

Wave-breaking is another critical dissipation process of ocean waves, which is highly intermittent but simultaneous with wave-generated turbulence stated above. However, the former mechanism still remains not well-understood (Donelan and Yuan, 1994; Young and Babanin, 2006; Yuan et al., 2009). Here in this study, based on the breaking wave statistical method that Cartwright and Longuet-Higgins (1956), Longuet-Higgins (1957), Yuan et al (1986, 2009) employed under a narrow spectrum assumption for theoretical arguments, we present a more precise approach for estimation of the dissipation-due-to-breaking. Parameterization treatments of the dissipation source function under the assumption of balance between growth and dissipation are discarded, instead of which we derive an improved analytical postbreaking spectrum expression satisfying the kinematic and dynamic wave-breaking onset criterions.

420 The postbreaking wave spectrum, via the covariance of surface elevation which was assumed to be Gaussian and stationary, was expressed as (Yuan et al., 1986; Yuan et al., 1993; Donelan and Yuan, 1994)

$$E_b(k_1, k_2) = \alpha_b E(k_1, k_2) \quad (20)$$

425 and

$$\alpha_b = \left[1 - \left(\frac{\omega}{\omega_b} \right)^2 \left(\frac{2}{\pi} \right)^{1/2} \frac{1}{L} \exp\left(-\frac{L^2}{2}\right) \right]^2 \quad (21)$$

where $L^{-1} = \frac{\mu_4^{1/2}}{g/2}$ denotes the normalized *rms*

acceleration, $T_b = 2\pi \left(\frac{\mu_2}{\mu_4} \right)^{1/2} = 2\pi \left(\frac{\mu_0}{\mu_2} \right)^{1/2} \rho = \rho T_z$ and $\omega_b = \frac{2\pi}{T_b}$ denote the mean period

430 or mean frequency of wave maxima, T_z denotes the zero-crossing wave period; ρ denotes a parameter associated with the spectrum width parameter ε_{sp} , i.e.,

$$\rho^2 = \frac{\mu_2^2}{\mu_0 \mu_4} \quad (22)$$

$$\varepsilon_{sp}^2 = 1 - \rho^2$$

435 (23)

and μ_i , the *i-th* order moment of the wave spectrum. It should be noted that all the variables stated above are related to the incipient waves, not the postbreaking ones.

So the attenuation coefficient α_b is derived as (The derivation processes to the following Eqs. (24-27) are provided in Appendix C)

$$440 \quad \alpha_b = \left[1 - 4(2\pi)^{-1/2} \frac{\rho \omega^2 \mu_0^{1/2}}{g} \exp\left(-\frac{\rho^2}{8} \frac{g^2}{\mu_0 \omega_z^4}\right) \right]^2 \quad (24)$$

where $\omega_z = \left(\frac{\mu_2}{\mu_0} \right)^{1/2}$ denotes the mean zero-crossing wave frequency. The ratio of total energy loss due to wave-breaking is given by

$$r_b = \frac{\iint_{\bar{k}} E(k_1, k_2) dk_1 dk_2 - \iint_{\bar{k}} E_b(k_1, k_2) dk_1 dk_2}{\iint_{\bar{k}} E(k_1, k_2) dk_1 dk_2} \approx 8(2\pi)^{-1/2} \frac{\rho \bar{\omega}^2 \mu_0^{1/2}}{g} \exp\left(-\frac{\rho^2}{8} \frac{g^2}{\mu_0 \omega_z^4}\right)$$

445 (25)

where $\bar{\omega}$ denotes the mean wave frequency with $\bar{\omega} = (\frac{\mu_2}{\mu_0})^{1/2} = \omega_z$ here. Babanin (2006) analyzed the measurement records by Yefimov and Khristoforov (1971) and concluded that the breaking ratio of dominant waves was 0.01-0.4 %.

In the neighborhood of wave crests $\mu_0 \bar{\omega}^2 \sim \frac{1}{2} c_0^2$, where c_0 is the characteristic wave

450 speed with $c_0^2 = g^2 \frac{\mu_0^{1/2}}{\mu_4^{1/2}} \rho$ (Yuan et al., 2009), so

$$\frac{\bar{\omega}^2 \mu_0^{1/2}}{g} = \frac{\bar{\omega}^2 \mu_0}{g \mu_0^{1/2}} \sim \frac{c_0^2}{2g \mu_0^{1/2}} = \frac{g \mu_2}{2 \mu_0^{1/2} \mu_4} = \rho \frac{g}{2 \mu_4^{1/2}} = \rho L. \text{ This yields } r_b \sim \rho^2 L, \text{ which agrees}$$

with the relative mechanical energy loss per unit sea surface area. Yuan et al. (2009) derived some basic statistics of wave breaking for a narrow spectrum, especially the breaking kinetic and potential energy loss which add up to deduce the breaking
 455 mechanical energy loss formulated by introducing the ratio of the former to the latter. Wang et al. (2017, 2018) concluded that the ratio is mainly within the range 3-30, which indicates that there is a disproportion feature between the wave kinetic energy loss and potential one due to wave-breaking. Shi et al. (2025) validated the statistical wave-breaking model across multiple sites from the High Wind Speed Gas Exchange
 460 Study (HiWinGS), and concluded that the model is highly effective in capturing the dynamics of whitecap coverage across a range of high sea states. Based on the latest findings, an improved attenuation coefficient by introducing the breaking kinetic energy loss is proposed as follows:

$$\alpha'_b = 1 - \rho \frac{\omega^2 \mu_0^{1/2}}{g} \frac{1}{L} \left[L \int_{-\infty}^{-L} \exp\left\{-\frac{1}{2} Z^2\right\} dZ + \exp\left\{-\frac{\rho^2}{8} \frac{g^2}{\mu_0 \omega_z^4}\right\} \right]$$

465 (26)

where the first and second terms in the bracket on the right-hand side are related to the dimensionless breaking kinetic and potential energy loss respectively,

$$L = \frac{g}{2 \mu_4^{1/2}} = \frac{\rho}{\pi \lambda} \left(\frac{H_s}{\bar{L}} \right)^{-1} = \frac{\rho}{2} \frac{g}{\mu_0^{1/2} \omega_z^2}, \text{ mean wavelength } \bar{L} = \lambda \frac{g}{2\pi} T_z^2, \lambda = \frac{2}{3} \text{ or } 0.86 \text{ (Kinsman,}$$

2012; Yuan et al., 2009; Xu and Yu, 2001). There is a prominent consistency between
 470 Eq. (26) and Eq. (24) under some certain circumstances. Let

$$\theta \equiv L \int_{-\infty}^{-L} \exp\left\{-\frac{1}{2} Z^2\right\} dZ \Big/ \exp\left\{-\frac{\rho^2}{8} \frac{g^2}{\mu_0 \omega_z^4}\right\}$$

represents the ratio of the kinetic energy loss to the potential one due to wave-breaking (Yuan et al., 2009; Wang et al., 2017, 2018), Eq. (26) can be rewritten as

$$\alpha'_b = 1 - \rho \frac{\omega^2 \mu_0^{1/2}}{g} \frac{1 + \theta}{L} \exp\left\{-\frac{\rho^2}{8} \frac{g^2}{\mu_0 \omega_z^4}\right\}$$

475 (27)

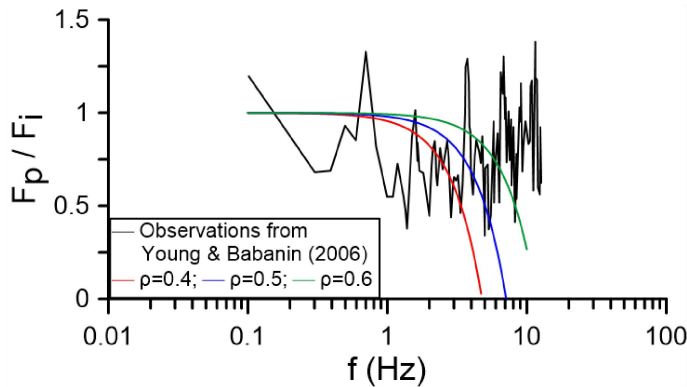
Suppose that $\frac{H_s}{L} = \frac{1}{7}, \rho = 0.6, \theta = 4$, then $\frac{1 + \theta}{L} \doteq 3.216 \sim 8(2\pi)^{-1/2} \doteq 3.192$, while

the latter coefficient comes originally from the complicated 0-1st order asymptotic expansions of the covariance of surface elevation, i.e. the foundation of the wave-breaking dissipation source function of the original MASNUM wave model.

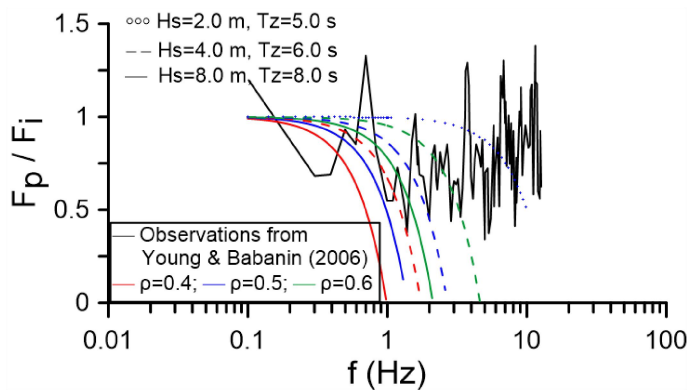
480 Equations (26) and (27) demonstrate definitely the dominant role of the kinetic energy loss induced by wave-breaking, and the former is applied in the following numerical experiments.

Young and Babanin (2006) obtained the breaking spectrum and nonbreaking spectrum from segments of the comprehensive measurement records in the Australian
 485 Shallow Water Experiment (AUSWEX), carried out at Lake George in New South Wales in 1997-2000, and analyzed the spectral difference with the ratio of the two spectra plotted as a function of frequency f in Fig. 5. According to Eq. (26), we also calculate the attenuation coefficient with $H_s = 0.45$ m, $f_p = 0.39$ Hz but ρ differs from 0.4 to 0.6. Although there is oscillation mainly caused by survey array of high-
 490 precision capacitance wave probes, a decreasing tendency of the “observed” ratio is remarkable from low frequencies to the high frequency $f = 5f_p$, which imparts the fact that the longer wave scales are more affected by the dominant breaking. The calculated attenuation coefficients correspond to this tendency, which yields valuable insights of the physics of dominant breaking, but the statistical approach is less well-
 495 suited for simulating the rapid transient regime of wave breaking as well as for the higher frequency in the equilibrium range. For the higher frequency $f > 5f_p$, there is not the decreasing feature for the “observed” ratio, this can be explained by the

statistical equilibrium in the equilibrium range proposed by Phillips (1985) or the short scales' prompt recovery interpreted by Young and Babanin (2006). When Eq. (26) is applied in the 3rd generation wave models, e.g. the MASNUM wave model (Yuan et al, 1991; Yang et al., 2005), though the attenuation coefficient α'_b approaches to zero for those higher frequencies, the equilibrium wave spectra in the equilibrium range are used to complement the underestimation induced by wave-breaking.



505 **Figure 5.** Ratio of the spectra between incipient-breaking and postbreaking waves. Black line: Observations are digitalized from Young and Babanin (2006); Color lines: Calculated α'_b according to Eq. (26) with $\rho=0.4, 0.5, 0.6$ respectively.



510 **Figure 6.** Same as Fig. 5 but for ordinary and high sea states. Observations digitalized from Young and Babanin (2006) are also displayed for comparison. Circles, dashed and solid lines represent different wave states, while colors represent different ρ selected in Eq. (26).

We further evaluate the attenuation coefficients by using Eq. (26) on ordinary and high sea states, which are plotted in Fig. 6. Apart from the significant wave height, the zero-crossing wave period also plays an important role for the quantity of the attenuation coefficient. In addition, it decreases apparently at high sea states, which indicates the wave-breaking intensity is more remarkable.

3 Application implementations on simple duration-limited growth and decay experiments

520 There remain two undetermined parameters α_{wt} , ρ in the preceding section, which will be discussed further in Section 4. Both of them are chosen as tunable parameters in the duration-limited growth and decay experiments undertaken below. The numerical experiments were carried out with the MASNUM wave model (Yuan et al, 1991; Yang et al., 2005), and implemented according to the studies of Janssen et al. 525 (1994). We ran the model for seven days, the first two days with a wind speed of 18.45 m s^{-1} , after which the wind dropped to a value of 5 m s^{-1} . The model integration time step was 30 s, so the growth limiter can be switched off and its impacts need not be considered here.

For simplicity, the parameterization of linear growth in spectral density proposed 530 by Komen et al. (1984) and the quasi-linear one by Janssen (1991) for wind input source function S_{in} are used respectively. As stated above, coefficient α_{wt} should be tuned to 0.02 - 0.2. Wang et al. (2017, 2018) validated the sea surface whitecap coverage obtained from the statistical wave-breaking model with the satellite-derived data and proposed that the range of ρ is 0.53 - 0.59, and this referenced span is used 535 in the following experiments.

To evaluate the scaling behavior of the new dissipation formulations due to wave-generated turbulence and wave-breaking proposed in Section 2, as well as their different effects, several numerical experiments are carried out (Table 2). In the original 3rd generation MASNUM wave model described here (Experiment 1), a 540 parameterization proposed by Yuan et al. (1986), Yuan et al. (1993), Donelan and Yuan (1994) is adopted for wave-breaking dissipation source function S_{ds} , i.e.,

$$S_{ds} = -d_1 \hat{\omega} \left(\frac{\omega}{\hat{\omega}} \right)^2 \left(\frac{\hat{\alpha}}{\hat{\alpha}_{PM}} \right)^{1/2} \exp \left\{ -d_2 (1 - \varepsilon_{sp}^2) \frac{\hat{\alpha}_{PM}}{\hat{\alpha}} \right\} E(k_1, k_2) \quad (28)$$

where $\hat{\omega} = (\mu_{-1} / \mu_0)^{-1}$, $\hat{\alpha} = \mu_0 \hat{\omega}^4 g^{-2}$, $\hat{\alpha}_{PM}$ is the value of $\hat{\alpha}$ for a PM spectrum 545 ($\hat{\alpha}_{PM} = 3.02 \times 10^{-3}$). Two critical coefficients d_1 and d_2 ($d_1 = 1.32 \times 10^{-4}$, $d_2 = 2.61$) were retrieved through fitting algorithm with the dimensional expression proposed by

Komen et al. (1984). The corresponding dissipation term in the WAM-Cycle models is given as.

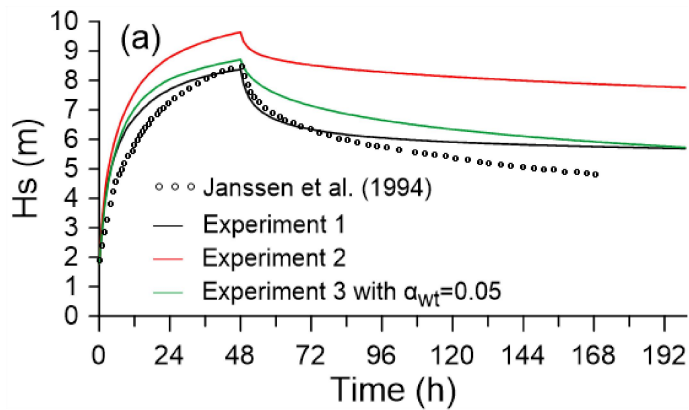
$$S_{ds} = -C_{ds} \bar{\omega} \left(\frac{\omega}{\bar{\omega}} \right)^2 \left(\frac{\hat{\alpha}}{\hat{\alpha}_{PM}} \right)^2 E(k_1, k_2) \quad (29)$$

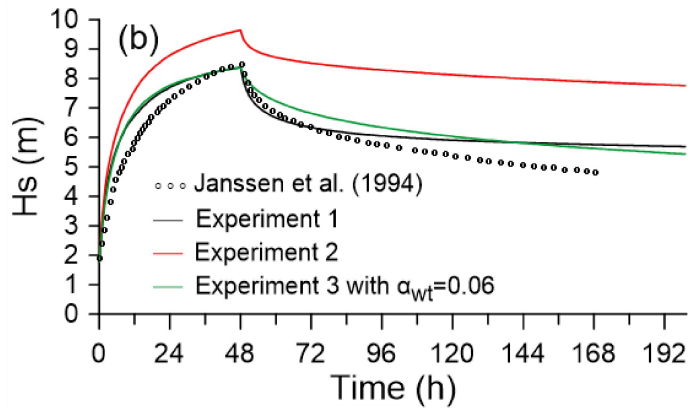
550 where C_{ds} is a constant ($C_{ds} = 2.36 \times 10^{-5}$).

In Experiment 2, instead of this source function S_{ds} , Eqs. (20) and (26) are used to calculate the postbreaking spectrum, while other unchanged source functions S_{in} , S_{nl} , S_{bo} and S_{cu} are integrated to obtain the incipient-breaking spectrum. Then the dissipation source function induced by wave-generated turbulence S_{tid} is further
 555 considered in Experiment 3. In the above Experiments 2 and 3, $\rho = 0.59$ is chosen, while $\rho = 0.53$ in the supplemental Experiment 2S for further comparison.

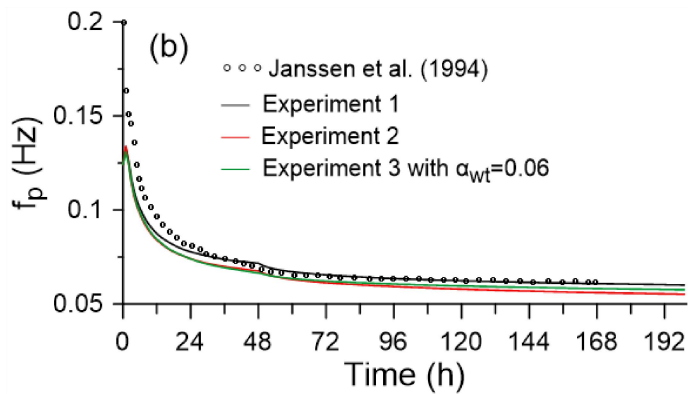
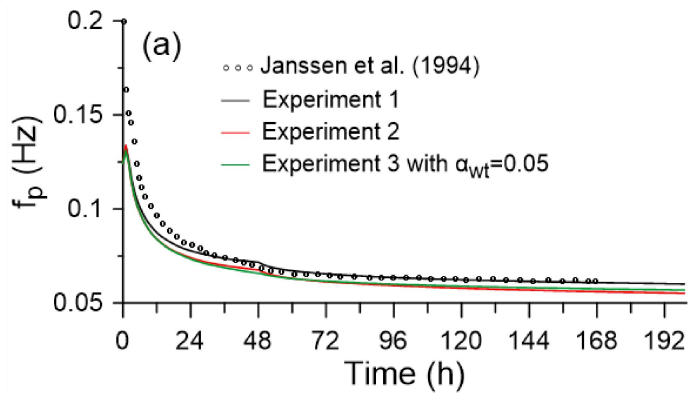
Experiment number	Original S_{ds}	Equations (20) and (26) (Improved postbreaking spectrum $E_b(k_1, k_2)$)	Equation (15) (Dissipation source function S_{tid} induced by wave-generated turbulence)
1	√	×	×
2	×	√ ($\rho = 0.59$)	×
2S	×	√ ($\rho = 0.53$)	×
3	×	√ ($\rho = 0.59$)	√

Table 2. Numerical experiments





560 **Figure 7.** Time evolution of wave height over a seven day period. Modeled data (circles) are digitalized from Janssen et al. (1994). After two days the wind drops. Notice the decay in wave height during the last five days when the waves are considered as swell. **(a)** $\alpha_{wt} = 0.05$; **(b)** $\alpha_{wt} = 0.06$.



565 **Figure 8.** Time evolution of peak frequency over a seven day period. Modeled data (circles) are digitalized from Janssen et al. (1994). After two days the wind drops. Notice the decay in the slight shift in peak frequency during the last five days when the waves are considered as swell. **(a)** $\alpha_{wt} = 0.05$; **(b)** $\alpha_{wt} = 0.06$.

570 Figures 7 and 8 show the time evolutions of wave height and peak frequency, where the wind input source function in MASNUM wave model was adopted from Komen et al. (1984). The wave height grows during the first two days, then decreases significantly after the wind drops two days later. Results of Janssen et al. (1994) with

circle symbols are listed for comparison with Experiment 1-3. Results of the original
 575 MASNUM wave model (Experiment 1) are consistent with that of Janssen et al.
 (1994), but the deviation of wave height may be noted 96h later due to different
 power of normalized wave slope in the wave-breaking dissipation source function
 (Yuan et al., 1991; Donelan and Yuan, 1994). The difference of wave height between
 Experiment 2 and others, both the maximum quantity and swell decay, can be
 580 distinguished apparently. Especially the wave height in Experiment 2 hardly changes
 during the swell decay process, because the mean swell steepness becomes small
 gradually and $\alpha'_b \sim 1.0$ in Eqs. (20) and (26). This indicates that the wave energy loss
 induced by wave-breaking is inadequate, and the role of prior proposed
 parameterizations for wave-breaking dissipation may be overestimated in the previous
 585 studies. Besides the effect of postbreaking wave spectrum, the dissipation source
 function induced by wave-generated turbulence S_{tid} is incorporated in Experiment 3.
 The corresponding modeled wave height and peak frequency are also listed in Figs. 7
 and 8, in which different $\alpha_{wt} = 0.05$ or 0.06 is selected to highlight its effect.
 Discrepancies for the maximum of wave height and swell decay are reduced much
 590 than that of Experiment 2, and its variation has an analogous trend with that of
 Janssen et al. (1994).

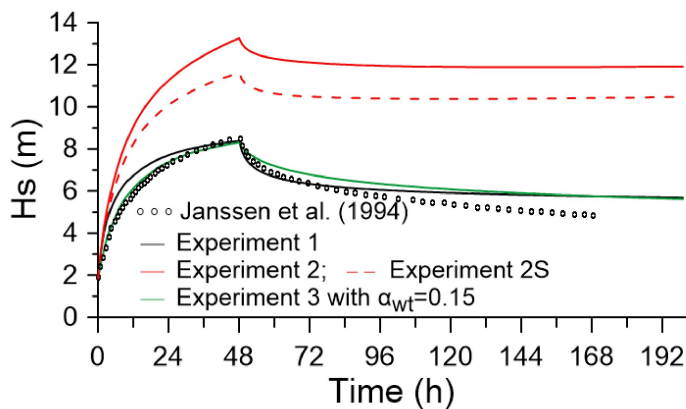


Figure 9. Same as Fig. 7 but the wind input source function in MASNUM wave model was adopted from Janssen (1991) and $\alpha_{wt} = 0.15$.

595 Figure 9 shows the time evolution of wave height, where the wind input source function in MASNUM wave model was adopted from Janssen (1991). Similar interpretation stated above can be obtained, besides that the effect of postbreaking wave spectrum is still inadequate even for that in the supplemental Experiment 2S where $\rho = 0.53$.

600 **4 Discussions**

The analytical approaches and the corresponding comparisons to laboratory or in-lake site measurements improve further understandings of wave energy dissipation due to wave-breaking and wave-generated turbulence. This study still exhibits some deficiencies and needs to be addressed on comparative assessments and metrics to previous formulations, as well as evaluations of scaling behavior of the new model, etc. Model validation is tentative and requires future enhanced observations correspondingly. Moreover, there remain problems to be addressed that ρ , α_{wt} are chosen as constants in this study. Parameter ρ is associated with the spectrum width ε . And according to the statistical theory of breaking waves (Cartwright and Longuet-Higgins, 1956; Longuet-Higgins, 1957; Yuan et al., 1986, 2009), both parameters ρ , ε should be referred to those of incipient-breaking spectrum, which is obtained as an intermediate variable in our model where all source functions are integrated except for the energy loss induced by wave-breaking. In fact, the observed or model outputted wave spectrum would respond to the postbreaking wave spectrum (Donelan and Yuan, 1994). So the prior-to-breaking parameter ρ or ε is currently still poorly understood. Moreover, Lamarre and Melville (1991), Melville et al. (1992) showed that 30% - 50% of energy lost by breaking waves is expended on entraining bubbles into the water against buoyancy forces, and the residue contributes to the turbulence generation. The interaction mechanism of the breaking-induced turbulence with the progressive waves is also unknown. It should also be mentioned that the whitecap model originally proposed by Hasselmann (1974) is an after-breaking class model, and its inherent assumptions need experimental verification (Young and Babanin, 2006). The whitecaps are situated on the forward faces of the waves, exert a downward pressure on the upward moving water, but the direct and precise estimates of their negative work on the waves need further studies. Given the intricate interactions state above, in our model proposed here, the choice of ρ as a tuned parameter is tentative for numerical implementation.

The constant α_{wt} is chosen in such a way as a tuned coefficient that it implies the quasi-equilibrium level of wave-generated turbulence, and physically it depends on the normalized shear instability strength of wave motion and further relates to the normalized 3rd-order moment of wave spectrum (see also Eqs. 7-8). Therefore it is

certainly not constant at any instant t in real-world scenarios and its reasonable parameterization should be further studied in the future. This idea is quite similar to the wave-amplitude-based Reynolds number proposed by Babanin (2006), its critical wave Reynolds number for wave-induced turbulence can reach down to a lower margin, $Re_{\text{wave}} \sim 1000$, from a series of laboratory experiments (Babanin and Haus, 2009; Dai, et al., 2010). But the appropriate dissipation rate for model implements cannot be inferred from the wave Reynolds number alone and was approached by experimental means (Babanin, 2011; Zieger et al., 2015; Liu, et al., 2019). The gradient Richardson number R_g may be a more appropriate dependency factor for the coefficient α_{wt} , which needs further perspectives. If the gradient Richardson number R_g is smaller than a critical value R_g^c , instability of the flow occurs, i.e.,

$$R_g = \frac{\hat{N}_3^2}{\left| \frac{\partial u_{\text{SM}\alpha}}{\partial x_3} \right|^2} < R_g^c, \quad \alpha = 1, 2$$

where $\hat{N}_3^2 = -g \frac{\partial}{\partial x_3} \left(\frac{\hat{\rho}}{\rho_0} \right)$, the Brunt–Väisälä frequency. Below we let

$\hat{N}_3 = \text{const} \approx 0.01 \text{ rad s}^{-1}$ in the upper layers and the critical value $R_g^c \approx 1/2$ (Baumert and Peters, 2000; Baumert et al., 2005). For a monochromatic non-breaking wave $\zeta = \eta \cos(k_\alpha x_\alpha - \omega t)$, which is deemed as a base motion in the framework of the ocean dynamic system, the instability criterion is simplified as

$$\hat{N}_3^2 < R_g^c \omega^2 (AK)^2 \exp(2Kx_3) \cos^2(k_\alpha x_\alpha - \omega t)$$

We roughly estimate the critical instability depth induced by the monochromatic waves (Table 3), Fig. 10 shows the dependence of the gradient Richardson number versus layer depth for Case 1 in Table 3. Below the wave crests and troughs, there exist bowl-shaped instability regions, which agree to the experimentally observed instantaneous turbulence incurred intermittently at the rear face of the progressive wave profile, but the breaking-in-progress turbulence develops at the front face (Babanin and Haus, 2009; Babanin, 2011). The coefficient α_{wt} is qualitatively related to the two-dimensional instability area proportion as shown in Fig. 10 or the instability volume proportion beneath the wave surface in real scenarios, which requires further research.

No.	Circular frequency ω (rad s ⁻¹)	Wave steepness AK	Wavenumber K (rad m ⁻¹)	Critical instability depth x_3^c (m)
1	1.0	0.1	0.1	19.6
2	1.0	0.3	0.1	30.5
3	0.63	0.1	0.04	37.2
4	0.63	0.05	0.04	19.9

Table 3. Critical instability depth induced by the monochromatic waves

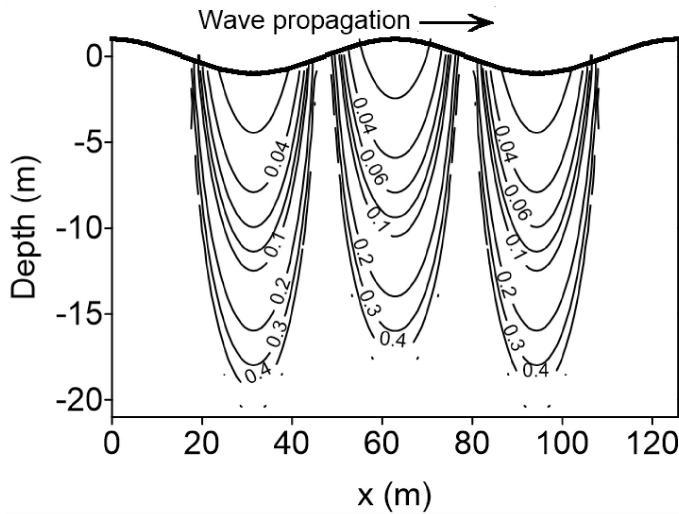


Figure 10. Dependence of the gradient Richardson number versus layer depth for Case 1 in Table 3.

665 Finally, some limitations of underlying assumptions in our theoretical arguments require further discussions. In the $k - \epsilon$ type eddy viscosity model of wave-generated turbulence, the turbulence timescale is assumed to be shorter than wave period. Therefore, the interaction of turbulence at other scales with ocean waves, which also accounts for a significant fraction of the energy losses of the wave field, is not
670 included in our practical numerical wave model. The quasi-equilibrium assumption of wave-generated turbulence poses the problem of an undetermined coefficient, which needs further elaborations especially essential precise measurements. The linear non-breaking wave theory applied to construct analytical solutions for the turbulence generation is an acceptable assumption in the general case of weakly nonlinear

675 situations, and the scale estimation via the shear instability of wave orbital motions
only represents a major portion of the turbulent production in the upper ocean. As
stated by Yuan et al. (2009), since the wave spectrum in real-world scenarios is not
actually narrow, the breaking wave statistical method under a narrow spectrum
assumption is not precise enough to estimate the attenuation coefficient for the
680 postbreaking wave spectrum.

5 Conclusions

The ocean wave energy dissipation is the least understood of the major source terms,
previous approaches to estimate the dissipation source function depended on an
685 incomplete description of the physics of the processes including wave-breaking and
wave-turbulence interaction. The latest observational efforts offer a possible approach
to explore the underlying comprehensive mechanisms.

In the present paper, we attempted to explore the dissipation effects of wave-
generated turbulence reacting on ocean waves, and to estimate the energy loss due to
690 wave-breaking via an improved postbreaking spectrum expression based on the
breaking wave statistical method. Two new source functions for the above two
dissipation processes are proposed and compared respectively to the laboratory or in-
lake observations tentatively in section 2, and their different dissipation effects are
experimentally analyzed in section 3.

695 The main conclusion of the study is that we propose an analytical dissipation
source function induced by wave-generated turbulence S_{tid} formulated by Eq. (15),
together with an improved postbreaking spectrum expression $E_b(k_1, k_2)$ by Eqs. (20)
and (26). The former dissipation term represents the feedback of imparting of wave
shear instability generations on turbulence, and the latter expression depicts the
700 intermittent wave-breaking events. Sum of both contributions play critical role of
wave energy dissipation.

Here in this paper we roughly estimate the effects of the above two dissipation
mechanisms in simple duration-limited growth and decay experiments. Calibration
and verification against a series of academic and realistic simulations, including the
705 fetch/duration-limited cases, turning wind (e.g. cold waves or monsoon) / rotatory

wind (e.g. extratropical or tropical cyclone) conditions, numerical hindcast and operational forecast in regional and global oceans, will be pursued in our future project, together with considering other concerned dissipation mechanisms.

710 *Code and data availability.* The MASNUM wave model can be downloaded at
<https://doi.org/10.5281/zenodo.19229991> (Yang et al., 2026), all configuration scripts,
pre-processing, and post-processing subroutines are included in the repository. Data
generated and analyzed during this study, as well as the processing code, can be
downloaded at <https://doi.org/10.5281/zenodo.19230125> (Sun et al., 2026). Other
715 data are available in the tables in the corresponding sections.

Author contributions. Conceptualization: YY, XY. Methodology: YY, FW, XJ.
Software: FW, XY, YY. Validation: YY, FW, XJ. Formal analysis: FW, YY, MS.
Investigation: MS, YY. Resources: MS, YS. Data curation: YS, MS. Writing—
720 original draft preparation: YY, MS. Writing—review and editing: FW, YT, XY, YS.
Visualization: MS, YS. Supervision: XJ, XY. Project administration: YS. Funding
acquisition: MS, YY.

Competing interests. The authors declare that they have no conflict of interest.

725

Acknowledgments. We especially thank distinguished supervisors for their opinion
and expertise given in the seminar series of the Ocean Dynamic System Team in the
MASNUM Lab.(Yuan et al., 2012, 2013). We also appreciate the comprehensive
WW3DG user manual and useful WAVEWATCH III software packages (WW3DG,
730 2019) for reference to improve our operational FORTRAN source codes. We
sincerely thank the anonymous reviewers for their thoughtful review and constructive
feedback, as well as the editors for their diligent work and valuable guidance.

Financial support. This research was jointly supported by the National Key Research
735 Program of China, under grant nos. 2023YFC3008200 and 2022YFC3104800; The
National Program on Global Change and Air-Sea Interaction (Phase II), under grant
no. GASI-04-WLHY-02 and Laoshan Laboratory Fund, under grant no.
LSKJ202203003.

740 **Appendix A**

Brief derivation of Eq. (1)

In the comprehensive framework of the ocean dynamic system comprised of wave-like motions, eddy-like motions and circulation, which are controlled by dynamic gravity balance, static gravity balance and geotropic balance respectively, ocean turbulence, highly random perturbations due to strong nonlinear advections in the foregoing three sub-systems, interacts with larger scale motions including the advection transport and shear instability generation of large-scale dynamic processes as well as the mixing effect in the form of its transport flux residual on the latter (Yuan et al., 2012; Yuan, 2024). More comprehensive governing equations for wave motion were derived under the assumption that turbulence timescale is much shorter than wave period and formulated in tensor expression as follows (Yuan et al., 2012; Yuan, 2024):

$$\frac{\partial u_{SMj}}{\partial x_j} = 0 ,$$

755 (A1)

$$\begin{aligned} & \frac{\partial u_{SMi}}{\partial t} + \hat{U}_j \frac{\partial u_{SMi}}{\partial x_j} + u_{SMj} \frac{\partial \hat{U}_i}{\partial x_j} + \frac{\partial}{\partial x_j} (u_{SMj} u_{SMi} - \langle u_{SMj} u_{SMi} \rangle_{SM}) - 2\varepsilon_{ijk} u_{SMj} \Omega_k \\ & = -\frac{1}{\rho_0} \frac{\partial p_{SM}}{\partial x_i} - g \frac{\rho_{SM}}{\rho_0} \delta_{3i} + \frac{\partial}{\partial x_j} \left(\nu_0 \frac{\partial u_{SMi}}{\partial x_j} \right) + \frac{\partial}{\partial x_j} \left[- \left(\langle u_{SSj} u_{SSi} \rangle_{SS} - \langle \langle u_{SSj} u_{SSi} \rangle_{SS} \rangle_{SM} \right) \right] , \end{aligned}$$

(A2)

$$\begin{aligned} & \frac{\partial \rho_{SM}}{\partial t} + \hat{U}_j \frac{\partial \rho_{SM}}{\partial x_j} + u_{SMj} \frac{\partial \hat{\rho}}{\partial x_j} + \frac{\partial}{\partial x_j} (u_{SMj} \rho_{SM} - \langle u_{SMj} \rho_{SM} \rangle_{SM}) \\ & = \frac{\partial}{\partial x_j} \left(K_0 \frac{\partial \rho_{SM}}{\partial x_j} \right) + \frac{\partial}{\partial x_j} \left[- \left(\langle u_{SSj} \rho_{SS} \rangle_{SS} - \langle \langle u_{SSj} \rho_{SS} \rangle_{SS} \rangle_{SM} \right) \right] + Q_{\rho SM} , \end{aligned} \tag{A3}$$

760 where $u_{SMi}, i = 1, 2, 3; \rho_{SM}$ denote the ocean wave components, $\hat{U}_i, i = 1, 2, 3; \hat{T}, \hat{s}, \hat{p}, \hat{\rho}$ denote the background current components, ρ_0 is the basin mean water density; ν_0, K_0, D_0 denote the molecular viscosity, thermal and diffusion coefficients; $Q_{\rho SM}$ denotes the thermal source due to temperature and salinity perturbations; $\langle \cdot \rangle_{SS}$,

$\langle \cdot \rangle_{SM}$ denote the Reynolds averages on the turbulence and wave motions

765 respectively. Hereafter, other symbols have their usual meaning.

Multiplying Eq. (A2) by $\rho_0 u_{SMi}$ and Eq. (A3) by ρ_{SM} , after some manipulation, yields the unit volume mechanical kinetic energy and potential energy respectively. Sum of both energy terms and Reynolds averaged on the wave motion reduce to

$$\begin{aligned}
& \frac{\partial}{\partial t} \left\langle \frac{\rho_0 u_{SMi}^2}{2} + \frac{g^2 \rho_{SM}^2}{2 \rho_0 \hat{N}_3^2} \right\rangle_{SM} + \left\langle (\hat{U}_j + u_{SMj}) \frac{\partial}{\partial x_j} \left(\frac{\rho_0 u_{SMi}^2}{2} + \frac{g^2 \rho_{SM}^2}{2 \rho_0 \hat{N}_3^2} \right) \right\rangle_{SM} + \frac{\partial}{\partial x_i} \langle p_{SM} u_{SMi} \rangle_{SM} \\
& = -\rho_0 \langle u_{SMi} u_{SMj} \rangle_{SM} \frac{\partial \hat{U}_i}{\partial x_j} + g \langle \rho_{SM} u_{SM\beta} \rangle_{SM} \frac{\hat{N}_\beta^2}{\hat{N}_3^2} + \frac{g^2}{\rho_0 \hat{N}_3^2} \langle \rho_{SM} Q_{\rho SM} \rangle_{SM} \\
& + \left[\left\langle \rho_0 u_{SMi} \frac{\partial}{\partial x_j} \left(v_0 \frac{\partial u_{SMi}}{\partial x_j} \right) \right\rangle_{SM} + \left\langle \frac{g^2 \rho_{SM}}{\rho_0 \hat{N}_3^2} \frac{\partial}{\partial x_j} \left(K_0 \frac{\partial \rho_{SM}}{\partial x_j} \right) \right\rangle_{SM} \right] \\
& + \left[\left\langle \rho_0 u_{SMi} \frac{\partial}{\partial x_j} (-\langle u_{SSj} u_{SSi} \rangle_{SS}) \right\rangle_{SM} + \left\langle \frac{g^2 \rho_{SM}}{\rho_0 \hat{N}_3^2} \frac{\partial}{\partial x_j} (-\langle u_{SSj} \rho_{SS} \rangle_{SS}) \right\rangle_{SM} \right] \quad , \quad (A4)
\end{aligned}$$

770 Based on closure assumptions of the $k - \varepsilon$ type eddy viscosity model (Baumert et al., 2005; Yuan et al., 2013), Eq. (A4) can be written as

$$\begin{aligned}
& \frac{\partial}{\partial t} \left\langle \frac{\rho_0 u_{SMi}^2}{2} + \frac{g^2 \rho_{SM}^2}{2 \rho_0 \hat{N}_3^2} \right\rangle_{SM} + \left\langle (\hat{U}_j + u_{SMj}) \frac{\partial}{\partial x_j} \left(\frac{\rho_0 u_{SMi}^2}{2} + \frac{g^2 \rho_{SM}^2}{2 \rho_0 \hat{N}_3^2} \right) \right\rangle_{SM} + \frac{\partial}{\partial x_i} \langle p_{SM} u_{SMi} \rangle_{SM} \\
& = \left(-\rho_0 \langle u_{SMi} u_{SMj} \rangle_{SM} \frac{\partial \hat{U}_i}{\partial x_j} + g \langle \rho_{SM} u_{SM\alpha} \rangle_{SM} \frac{\hat{N}_\alpha^2}{\hat{N}_3^2} + \frac{g^2}{\rho_0 \hat{N}_3^2} \langle \rho_{SM} Q_{\rho SM} \rangle_{SM} \right. \\
& \left. + \left[\frac{\partial}{\partial x_j} \left\langle \left(v_0 + \frac{k^2}{\pi^2 \varepsilon} \right) \frac{\partial}{\partial x_j} \left(\frac{\rho_0 u_{SMi}^2}{2} \right) \right\rangle_{SM} + \frac{\partial}{\partial x_j} \left\langle \left(K_0 + \frac{1}{\sigma_0} \frac{k^2}{\pi^2 \varepsilon} \right) \frac{\partial}{\partial x_j} \left(\frac{g^2 \rho_{SM}^2}{2 \rho_0 \hat{N}_3^2} \right) \right\rangle_{SM} \right] \right. \\
& \left. + \left[-\left\langle \rho_0 \left(v_0 + \frac{k^2}{\pi^2 \varepsilon} \right) \left(\frac{\partial u_{SMi}}{\partial x_j} \right)^2 \right\rangle_{SM} - \left\langle \frac{g^2}{\rho_0 \hat{N}_3^2} \left(K_0 + \frac{1}{\sigma_0} \frac{k^2}{\pi^2 \varepsilon} \right) \left(\frac{\partial \rho_{SM}}{\partial x_j} \right)^2 \right\rangle_{SM} \right] \right) \quad (A5)
\end{aligned}$$

where $\hat{N}_i^2 = -g \frac{\partial}{\partial x_i} \left(\frac{\hat{\rho}}{\rho_0} \right)$, $i = 1, 2, 3$ denote the Brunt-Väisälä frequency components;

775 $\sigma_0 = \frac{1}{2}$ the Prandtl number; k, ε the kinetic energy and the dissipation rate of ocean turbulence, which is generated by shear instability of background current, Stokes drift and wave orbital motions in the upper layers. Here in this study, only the wave-generated turbulence is considered. Its analytical mixing coefficients were proposed through equilibrium solutions of the second-order turbulence closure model between
780 the wave motion shear instability generations and the TKE dissipations (Yuan et al., 2013).

Appendix B

Brief derivations of Eq. (12), Eq. (15) and Eq. (19)

785 Yuan et al. (2013) proposed equilibrium solutions of the $k - \varepsilon$ type eddy viscosity model from the minimization relation, and the TKE dissipation rate ε can be expressed as

$$\bar{\varepsilon} \approx \frac{7}{8} \frac{\bar{k}^2}{\pi^2 \bar{\varepsilon}} \left(\frac{\partial u_{SMi}}{\partial x_j} \right)^2$$

(B1)

790 The approximate coefficient 7/8 indicates that the shear instability generation of surface waves is the dominant source of the turbulence in the upper ocean. Based the mixing length of $\bar{l}_D = \frac{\bar{k}^{-3/2}}{\pi^{3/2} \bar{\varepsilon}}$ (Baumert et al., 2005), \bar{k} , $\bar{\varepsilon}$ are formulated conveniently as

$$\bar{k} = \frac{7}{8} \pi \bar{l}_D^2 \left(\frac{\partial u_{SMi}}{\partial x_j} \right)^2$$

$$\bar{\varepsilon} = \left(\frac{7}{8} \right)^{3/2} \bar{l}_D^2 \left(\left| \frac{\partial u_{SMi}}{\partial x_j} \right| \right)^3$$

795 Then the mixing coefficient $\left\langle \frac{\bar{k}^2}{\pi^2 \bar{\varepsilon}} \right\rangle_{SM}$ is expressed as

$$\left\langle \frac{\bar{k}^2}{\pi^2 \bar{\varepsilon}} \right\rangle_{SM} = \left(\frac{7}{8} \right)^{1/2} \left\langle \bar{l}_D^2 \right\rangle_{SM} \left\langle \left| \frac{\partial u_{SMi}}{\partial x_j} \right| \right\rangle_{SM}$$

(B2)

Yuan et al. (2013) discussed the relation of the classical Prandtl mixing-length theory (Yuan et al., 1999) with the equilibrium solution of the $k - \varepsilon$ type eddy viscosity
800 model by the available 12 groups of field data measurements. Here in this study, only the wave-generated turbulence is considered, so we let

$$\bar{l}_D \approx \left| \iint_{\bar{k}} A \frac{\cosh K(\hat{H} + x_3)}{\sinh K\hat{H}} \exp \left\{ i(\bar{\mathbf{k}} \cdot \bar{\mathbf{r}} - \omega t) \right\} d\bar{\mathbf{k}} \right|$$

(B3)

where the wavenumber vector $\bar{\mathbf{k}} = (k_1, k_2)$ with $K = \sqrt{k_1^2 + k_2^2}$, $\bar{\mathbf{r}} = (x_1, x_2)$. ω

805 denotes the radian frequency, and A , the wave amplitude. $\langle \bar{I}_D^2 \rangle_{SM}$, $\left\langle \frac{\partial u_{SMi}}{\partial x_j} \frac{\partial u_{SMi}}{\partial x_j} \right\rangle_{SM}$ can be

expressed in wavenumber spectrum as

$$\langle \bar{I}_D^2 \rangle_{SM} \approx \iint_{\bar{\mathbf{k}}} E(k_1, k_2) \frac{\cosh^2 K(\hat{H} + x_3)}{\sinh^2 K\hat{H}} dk_1 dk_2$$

$$\left\langle \frac{\partial u_{SMi}}{\partial x_j} \frac{\partial u_{SMi}}{\partial x_j} \right\rangle_{SM} = \iint_{\bar{\mathbf{k}}} 2\omega^2 K^2 \frac{\cosh 2K(\hat{H} + x_3)}{\sinh^2 K\hat{H}} E(k_1, k_2) dk_1 dk_2$$

Then the mixing coefficient is reduced to

$$810 \quad \left\langle \frac{\bar{k}^2}{\pi^2 \bar{\varepsilon}} \right\rangle_{SM} = \frac{\sqrt{7}}{2} \iint_{\bar{\mathbf{k}}} E(k_1, k_2) \frac{\cosh^2 K(\hat{H} + x_3)}{\sinh^2 K\hat{H}} dk_1 dk_2 \left(\iint_{\bar{\mathbf{k}}} \omega^2 K^2 \frac{\cosh 2K(\hat{H} + x_3)}{\sinh^2 K\hat{H}} E(k_1, k_2) dk_1 dk_2 \right)^{1/2}$$

(B4)

which is Eq. (12) in Section 2.1.

For deep water depth, $\frac{\cosh K(\hat{H} + x_3)}{\sinh K\hat{H}} \sim \exp\{Kx_3\}$, $\frac{\cosh 2K(\hat{H} + x_3)}{\sinh^2 K\hat{H}} \sim 2\exp\{2Kx_3\}$, then Eq. (B4) is

reduced to

$$815 \quad \left\langle \frac{\bar{k}^2}{\pi^2 \bar{\varepsilon}} \right\rangle_{SM} = \frac{\sqrt{7}}{2} \iint_{\bar{\mathbf{k}}} E(k_1, k_2) \exp\{2Kx_3\} dk_1 dk_2 \left(\iint_{\bar{\mathbf{k}}} \omega^2 K^2 E(k_1, k_2) \exp\{2Kx_3\} dk_1 dk_2 \right)^{1/2}$$

(B5)

which is Eq. (13) in Section 2.1.

For future practical applications, we introduce some characteristic wavenumbers and frequencies for various integral mean variables, i.e.,

$$820 \quad \iint_{\bar{\mathbf{k}}} E(k_1, k_2) \exp\{2Kx_3\} dk_1 dk_2 \approx \exp\{2\hat{K}_1 x_3\} \iint_{\bar{\mathbf{k}}} E(k_1, k_2) dk_1 dk_2,$$

$$\iint_{\bar{\mathbf{k}}} \omega^2 K^2 E(k_1, k_2) \exp\{2Kx_3\} dk_1 dk_2 \approx \omega^2 \hat{K}_2^2 \exp\{2\hat{K}_2 x_3\} \iint_{\bar{\mathbf{k}}} E(k_1, k_2) dk_1 dk_2,$$

$$\iint_{\bar{\mathbf{k}}} \frac{1}{2K + 2\hat{K}_1 + \hat{K}_2} \omega^2 K^2 E(k_1, k_2) dk_1 dk_2 \approx \frac{1}{5\hat{K}_3} \iint_{\bar{\mathbf{k}}} \omega^2 K^2 E(k_1, k_2) dk_1 dk_2.$$

Here we assume that $\hat{K}_1 \approx \hat{K}_2 \approx \hat{K}_3 \approx \hat{K}$ approximately. After some algebraic procedures,

Eq. (B5) is reduced to

$$825 \quad \left\langle \frac{\bar{k}^2}{\pi^2 \bar{\varepsilon}} \right\rangle_{\text{SM}} \approx \sqrt{\frac{7}{2}} \hat{\omega} \hat{K} \left(\iint_{\hat{k}} E(k_1, k_2) dk_1 dk_2 \right)^{\frac{3}{2}} \exp\{3Kx_3\}$$

(B6)

which is Eq. (14) in Section 2.1. And by using the above unified $\hat{\omega}$, \hat{K} and employing Eq. (B6), Eq. (11) in Section 2.1 can be derived as

$$830 \quad S_{\text{tid}} \approx -\frac{2\sqrt{14}}{5} \alpha_{\text{wt}} K^3 \hat{\omega} \left(\iint_{\hat{k}} E(k_1, k_2) dk_1 dk_2 \right)^{\frac{3}{2}} E(k_1, k_2)$$

(B7)

which is Eq. (15) in Section 2.1 for our further convenient numerical applications.

For monochromatic non-breaking waves, the derivation processes are similar as above. For deep water depth, we have

$$\left\langle \bar{I}_D^2 \right\rangle_{\text{SM}} \approx \frac{1}{2} A^2 \exp(2Kx_3)$$

$$835 \quad \left\langle \frac{\partial u_{\text{SM}i}}{\partial x_j} \frac{\partial u_{\text{SM}i}}{\partial x_j} \right\rangle_{\text{SM}} = 2A^2 \omega^2 K^2 \exp(2Kx_3)$$

and

$$\left\langle \frac{\bar{k}^2}{\pi^2 \bar{\varepsilon}} \right\rangle_{\text{SM}} = \frac{\sqrt{7}}{4} A^3 \omega K \exp\{3Kx_3\}$$

By employing Eq. (B1), the TKE dissipation rate ε_{dis} can be derived as

$$840 \quad \varepsilon_{\text{dis}} \approx \alpha_{\text{wt}} \frac{7}{8} \left\langle \frac{\bar{k}^2}{\pi^2 \bar{\varepsilon}} \right\rangle_{\text{SM}} \left\langle \left(\frac{\partial u_{\text{SM}i}}{\partial x_j} \right)^2 \right\rangle_{\text{SM}} = \frac{7\sqrt{7}}{16} \alpha_{\text{wt}} A^5 \omega^3 K^3 \exp\{5Kx_3\}$$

(B8)

which is Eq. (19) in Section 2.1.

Appendix C

Brief derivations of Eqs. (24-27)

845 Assuming that the surface elevation is Gaussian and stationary and breaking occurs wherever the vertical acceleration of the surface exceeds the dynamic criterion (Longuet-Higgins, 1969; Yuan et al., 1986), the surface limited by breaking can be

expressed by the Heaviside unit step function, and the postbreaking wave spectrum, via the complicated 0-1st order asymptotic expansions of the Fourier-domain covariance of surface elevation, can be formulated as Eq. (24) in Section 2.2 (Yuan et al., 1986; Hua and Yuan, 1992; Yuan et al., 1993):

$$\alpha_b = \left[1 - 4(2\pi)^{-1/2} \frac{\rho\omega^2\mu_0^{1/2}}{g} \exp\left(-\frac{\rho^2}{8} \frac{g^2}{\mu_0\omega_z^4}\right) \right]^2 \quad (C1)$$

where $\omega_z = (\frac{\mu_z}{\mu_0})^{1/2}$ denotes the mean zero-crossing wave frequency. Eq. (C1) can be expressed as

$$\alpha_b = 1 - 8(2\pi)^{-1/2} \frac{\rho\omega^2\mu_0^{1/2}}{g} \exp\left(-\frac{\rho^2}{8} \frac{g^2}{\mu_0\omega_z^4}\right) + \left[4(2\pi)^{-1/2} \frac{\rho\omega^2\mu_0^{1/2}}{g} \exp\left(-\frac{\rho^2}{8} \frac{g^2}{\mu_0\omega_z^4}\right) \right]^2 \quad (C2)$$

The third term on the right-hand side is a higher-order term compared to the second term, because the ratio of the two $r \sim \frac{\rho\omega^2\mu_0^{1/2}}{g} \sim \rho K \mu_0^{1/2} \sim \rho(AK)$, where $\rho^2 = 1 - \varepsilon_{sp}^2$, ε_{sp} denotes the spectrum width parameter and (AK) denotes the wave steepness. Then the third term is negligible, so the ratio of total energy loss due to wave-breaking is given by

$$r_b = \frac{\iint_{\bar{k}} E(k_1, k_2) dk_1 dk_2 - \iint_{\bar{k}} E_b(k_1, k_2) dk_1 dk_2}{\iint_{\bar{k}} E(k_1, k_2) dk_1 dk_2} \approx 8(2\pi)^{-1/2} \frac{\rho\bar{\omega}^2\mu_0^{1/2}}{g} \exp\left(-\frac{\rho^2}{8} \frac{g^2}{\mu_0\omega_z^4}\right) \quad (C3)$$

which is Eq. (25) in Section 2.2.

Yuan et al. (2009) incorporated the breaking surface elevation and the breaking criterion, then derived the breaking kinetic and potential energy loss which add up to deduce the breaking mechanical energy loss. The mechanical energy loss per unit time per unit sea surface area is formulated as

$$E_t = \frac{\rho_0 g \mu_0 \mu_4^{1/2}}{2\pi \mu_2^{1/2}} \rho^2 \left[L \int_{-\infty}^{-L} \exp\left\{-\frac{1}{2} Z^2\right\} dZ + \exp\left\{-\frac{\rho^2}{8} \frac{g^2}{\mu_0\omega_z^4}\right\} \right] \quad (C4)$$

(Here a slight correction is made to remove the coefficient $\sqrt{2}$ in the denominator in Eq. (54) of Yuan et al. (2009), this minor issue was introduced inadvertently in their Eq. (39) in which the coefficient 4 in the denominator is to be replaced with $2\sqrt{2}$.)

875 Considering the appropriate time scale $T_b = 2\pi(\frac{\mu_2}{\mu_4})^{1/2}$ associated with the loss of energy by wave breaking (Yuan et al., 1993; Donelan and Yuan, 1994), the mechanical energy loss per unit sea surface area is given by

$$\tilde{E} = T_b E_t = \rho_0 g \mu_0 \rho^2 \left[L \int_{-\infty}^{-L} \exp\left\{-\frac{1}{2}Z^2\right\} dZ + \exp\left\{-\frac{\rho^2}{8} \frac{g^2}{\mu_0 \omega_z^4}\right\} \right] \quad (C5)$$

880 In the neighborhood of wave crests $\mu_0 \bar{\omega}^2 \sim \frac{1}{2} c_0^2$, where $\bar{\omega}$ is the mean wave frequency, c_0 is the characteristic wave speed with $c_0^2 = g^2 \frac{\mu_0^{1/2}}{\mu_4} \rho$ (Yuan et al., 2009),

so $\frac{\bar{\omega}^2 \mu_0^{1/2}}{g} = \frac{\bar{\omega}^2 \mu_0}{g \mu_0^{1/2}} \sim \frac{c_0^2}{2g \mu_0^{1/2}} = \frac{g \mu_2}{2 \mu_0^{1/2} \mu_4}$. Then

$$\begin{aligned} \tilde{E} &= \rho_0 g \mu_0 \frac{\mu_2}{\mu_0^{1/2} \mu_4} \rho \left[L \int_{-\infty}^{-L} \exp\left\{-\frac{1}{2}Z^2\right\} dZ + \exp\left\{-\frac{\rho^2}{8} \frac{g^2}{\mu_0 \omega_z^4}\right\} \right] \\ &= \rho_0 g \mu_0 \frac{g \mu_2}{2 \mu_0^{1/2} \mu_4} \rho \frac{\mu_4^{1/2}}{g/2} \left[L \int_{-\infty}^{-L} \exp\left\{-\frac{1}{2}Z^2\right\} dZ + \exp\left\{-\frac{\rho^2}{8} \frac{g^2}{\mu_0 \omega_z^4}\right\} \right] \\ &= \rho_0 g \mu_0 \frac{g \mu_2}{2 \mu_0^{1/2} \mu_4} \rho \frac{1}{L} \left[L \int_{-\infty}^{-L} \exp\left\{-\frac{1}{2}Z^2\right\} dZ + \exp\left\{-\frac{\rho^2}{8} \frac{g^2}{\mu_0 \omega_z^4}\right\} \right] \\ &\sim \rho_0 g \iint_k \frac{\bar{\omega}^2 \mu_0^{1/2}}{g} \rho \frac{1}{L} \left[L \int_{-\infty}^{-L} \exp\left\{-\frac{1}{2}Z^2\right\} dZ + \exp\left\{-\frac{\rho^2}{8} \frac{g^2}{\mu_0 \omega_z^4}\right\} \right] E(k_1, k_2) dk_1 dk_2 \\ &\sim \rho_0 g \iint_k \frac{\omega^2 \mu_0^{1/2}}{g} \rho \frac{1}{L} \left[L \int_{-\infty}^{-L} \exp\left\{-\frac{1}{2}Z^2\right\} dZ + \exp\left\{-\frac{\rho^2}{8} \frac{g^2}{\mu_0 \omega_z^4}\right\} \right] E(k_1, k_2) dk_1 dk_2 \end{aligned} \quad (C6)$$

885 In the final step of the above manipulations, for the spectral wave fields, the mean wave frequency $\bar{\omega}$ should be replaced by ω to depict the localized wave breaking. Then the attenuation coefficient in the wavenumber space is formulated as:

$$\alpha'_b = 1 - \rho \frac{\omega^2 \mu_0^{1/2}}{g} \frac{1}{L} \left[L \int_{-\infty}^{-L} \exp\left\{-\frac{1}{2}Z^2\right\} dZ + \exp\left\{-\frac{\rho^2}{8} \frac{g^2}{\mu_0 \omega_z^4}\right\} \right] \quad (C7)$$

890 which is Eq. (26) in Section 2.2.

Let $\theta \equiv L \int_{-\infty}^{-L} \exp\left\{-\frac{1}{2}Z^2\right\} dZ / \exp\left\{-\frac{\rho^2}{8} \frac{g^2}{\mu_0 \omega_z^4}\right\}$ represents the ratio of the kinetic

energy loss to the potential one due to wave-breaking with a range of 3 to 30 (Yuan et al., 2009; Wang et al., 2017, 2018), Eq. (C7) can be rewritten as

$$\alpha'_b = 1 - \rho \frac{\omega^2 \mu_0^{1/2}}{g} \frac{1 + \theta}{L} \exp\left\{-\frac{\rho^2}{8} \frac{g^2}{\mu_0 \omega_z^4}\right\}$$

895 (C8)

which is Eq. (27) in Section 2.2.

Appendix D

Variable notation

900 As this study relies heavily on mathematical expressions, a list of symbols is provided in Table D1.

No.	Symbol	Notation
1	$x_i, i = 1, 2, 3$	Rectangular co-ordinate variables
2	$u_{SMi}, i = 1, 2, 3$	Wave velocity components
3	u_{w0}	Wave orbital velocity at sea surface
4	u^*	Friction velocity
5	τ_w, τ	Wave-induced stress and total stress
6	$\hat{N}_i, i = 1, 2, 3$	Brunt–Väisälä frequency components
7	k, ε	Turbulent kinetic energy (TKE) and TKE dissipation rate
8	$\bar{k}, \bar{\varepsilon}, \text{ and } \bar{l}_D$	Equilibrium variables of TKE and TKE dissipation rate, and mixing length
9	$e_{tid}, \varepsilon_{dis}$	Unit volume wave energy dissipation rate and TKE dissipation rate induced by wave-generated turbulence
10	ω	Wave radian frequency

11	A	Wave amplitude
12	\vec{k} , k_1 , k_2 and K	Wavenumber vector and wavenumber components with $\vec{k} = (k_1, k_2)$, wavenumber magnitude with $K = \sqrt{k_1^2 + k_2^2}$
13	C	Phase velocity with $C = \frac{\omega}{K}$
14	\hat{K}_1 , \hat{K}_2 , \hat{K}_3 , \hat{K} , and $\hat{\omega}$	Characteristic wavenumbers and frequency
15	$E(k_1, k_2)$	Wavenumber spectrum
16	μ_i	i -th order moment of the wave spectrum
17	ε_{sp} , ρ	Spectrum width parameter and parameter with $\rho = \sqrt{1 - \varepsilon_{sp}^2}$
18	T_b , ω_b , T_z and ω_z	Mean period and mean frequency of wave maxima with $\omega_b = \frac{2\pi}{T_b}$, mean zero-crossing wave period and wave frequency
19	$\bar{\omega}$ and c_0	Mean wave frequency and characteristic wave speed with $c_0 = \sqrt{g^2 \frac{\mu_0^{1/2}}{\mu_4^{1/2}} \rho}$ associated with breaking wave crests
20	$\hat{\omega}$	Mean wave frequency with $\hat{\omega} = (\mu_{-1} / \mu_0)^{-1}$

Table D1. Variable notation

REFERENCES

- 905 Alves, J. H. G., and Banner, M. L.: Performance of a saturation-based dissipation-rate source term in modeling the fetch-limited evolution of wind waves, *J. Phys. Oceanogr.*, 33, 1274-1298, [https://doi.org/10.1175/1520-0485\(2003\)033<1274:POASDS>2.0.CO;2](https://doi.org/10.1175/1520-0485(2003)033<1274:POASDS>2.0.CO;2), 2003.

Ardhuin, F., and Jenkins, A. D.: On the interaction of surface waves and upper ocean

- 910 turbulence, *J. Phys. Oceanogr.*, 36, 551-557, <https://doi.org/10.1175/JPO2862.1> ,
2006.
- Ardhuin, F., Chapron, B., and Collard, F.: Observation of swell dissipation across
oceans, *Geophys. Res. Lett.*, 36, L06607, <https://doi.org/10.1029/2008GL037030> ,
2009.
- 915 Ardhuin, F., Marié, L., Rasclé, N., Forget, P., and Roland, A.: Observation and
estimation of Lagrangian, Stokes, and Eulerian currents induced by wind and
waves at the sea surface, *J. Phys. Oceanogr.*, 39, 2820-2838,
<https://doi.org/10.1175/2009JPO4169.1>, 2009.
- Ardhuin, F., Rogers, W. E., Babanin, A. V., Filipot, J., Magne, R., Roland, A., van der
920 Westhuysen, A., Queff eulou, P., Lefevre, J., Aouf, L., and Collard, F.:
Semiempirical dissipation source functions for ocean waves. Part I: Definition,
calibration, and validation, *J. Phys. Oceanogr.*, 40, 1917-1941,
<https://doi.org/10.1175/2010JPO4324.1>, 2010.
- Babanin A. V.: On a wave-induced turbulence and a wave-mixed upper ocean layer,
925 *Geophys. Res. Lett.*, 33, L20605, <https://doi.org/10.1029/2006GL027308>, 2006.
- Babanin, A. V., Banner, M. L., Young, I. R., and Donelan, M. A.: Wave-follower field
measurements of the wind-input spectral function. Part III: Parameterization of the
wind-input enhancement due to wave breaking, *J. Phys. Oceanogr.*, 37, 2764-2775,
<https://doi.org/10.1175/2007JPO3757.1>, 2007.
- 930 Babanin, A. V.: Breaking of ocean surface waves, *Acta Phys. Slovaca*, 59(4), 305-535,
2009.
- Babanin, A. V., and Haus, B. K.: On the Existence of Water Turbulence Induced by
Nonbreaking Surface Waves, *J. Phys. Oceanogr.*, 39, 2675-2679,
<https://doi.org/10.1175/2009JPO4202.1> , 2009.
- 935 Babanin, A. V., Tsagareli, K. N., Young, I. R., and Walker, D. J.: Numerical
investigation of spectral evolution of wind waves. Part II: Dissipation term and
evolution tests, *J. Phys. Oceanogr.*, 40, 667-683,
<https://doi.org/10.1175/2009JPO4370.1>, 2010.
- Babanin, A. V.(Eds.): *Breaking and Dissipation of Ocean Surface Waves*, Cambridge
940 University Press, Cambridge, UK, 480pp., ISBN 978-1-107-00158-9,

<https://doi.org/10.1017/CBO9780511736162>, 2011.

- Babanin, A.V.: Swell attenuation due to wave-induced turbulence, in: Volume 2: Structures, safety and reliability. Proceedings of the 31st International Conference on Ocean, Offshore and Arctic Engineering, American Society of Mechanical Engineers, Rio de Janeiro, Brazil, 439-443, <https://doi.org/10.1115/OMAE2012-83706>, 2012.
- 945 Babanin A. V., and Chalikov, D.: Numerical investigation of turbulence generation in non-breaking potential waves, *J. Geophys. Res.*, 117, C00J17, <https://doi.org/10.1029/2012JC007929>, 2012.
- 950 Baumert, H., and Peters, H.: Second-moment closures and length scales for weakly stratified turbulent shear flows, *J. Geophys. Res.*, 105 (C3), 6453-6468, 2000.
- Baumert, H. Z., Simpson, J. H., and Sündermann, J. (Eds.): *Marine turbulence: theories, observations, and models*, Cambridge University Press, Cambridge, UK, 630pp., ISBN 978-0-521-15372-0, 2005.
- 955 Bidlot, J.-R.: Present status of wave forecasting at E.C.M.W.F., in: Proceedings of ECMWF workshop on ocean wave forecasting, June, 2012.
- Bidlot, J. R., Abdalla, S., and Janssen, P. A. E. M.: A revised formulation for ocean wave dissipation in CY25R1, Tech. Rep. Memorandum R60.9/JB/0516, Research Department, ECMWF, Reading, U. K., 2005.
- 960 Cartwright, D. E., and Longuet-Higgins, M. S.: The statistical distribution of the maxima of a random function, *Proc. Roy. Soc. London*, 237, 212–232, 1956.
- Chalikov, D.: The parameterization of the wave boundary layer, *J. Phys. Oceanogr.*, 25, 1,333-1,349 , 1995.
- Chalikov, D., and Babanin, A. V: Parameterization of wave boundary layer, *Atmosphere*, 2019, 10, 686, <https://doi.org/10.3390/atmos10110686>, 2019.
- 965 Chalikov, D. V., and Belevich, M. Y.: One-dimensional theory of the wave boundary layer, *Bound.-Layer Meteor.*, 63, 65–96, 1993.
- Collard, F., Ardhuin, F., and Chapron, B.: Monitoring and analysis of ocean swell fields from space: New methods for routine observations, *J. Geophys. Res.*, 114, C07023. <https://doi.org/10.1029/2008JC005215>, 2009.
- 970

- Dai, D., Qiao, F., Sulisz, W., and Han, L.: An experiment on the non-breaking surface-wave-induced vertical mixing, *J. Phys. Oceanogr.*, 40, 2180–2188, <https://doi.org/10.1175/2010JPO4378.1>, 2010.
- 975 Donelan, M. A., and Yuan, Y.: Wave dissipation by surface processes, in: *Dynamics and Modelling of Ocean Waves*, edited by: Komen, G. J., Cavaleri, L., Donelan, M., Hasselmann, K., Hasselmann, S., and Janssen, P. A. E. M., Cambridge University Press, Cambridge, UK, 143-155, ISBN 0-521-47047-1, 1994.
- Filipot, J. -F., and Ardhuin, F.: A unified spectral parameterization for wave breaking: from the deep ocean to the surf zone, *J. Geophys. Res.*, 117, C00J08, <https://doi.org/10.1029/2011JC007784>, 2012.
- 980 Grachev, A. A., and Fairall, C. W.: Upward momentum transfer in the marine boundary layer, *J. Phys. Oceanogr.*, 31, 1698 -1711, 2001.
- Guo, X., and Shen, L.: Numerical study of the effect of surface waves on turbulence underneath. Part 1. Mean flow and turbulence vorticity, *J. Fluid Mech.*, 733, 558-587, 2013.
- 985 Guo, X., and Shen, L.: Numerical study of the effect of surface waves on turbulence underneath. Part 2. Eulerian and Lagrangian properties of turbulence kinetic energy, *J. Fluid Mech.*, 744, 250-272, 2014.
- Hasselmann, K.: On the spectral dissipation of ocean waves due to whitecapping, *Bound.-Layer Meteor.*, 6, 107-127, 1974.
- 990 Hua F., and Yuan, Y.: Theoretical study of breaking wave spectrum and its application, *Sci. China Ser. B*, 9, 958-965, 1992.
- Huang, C., and Qiao, F.: Wave-turbulence interaction and its induced mixing in the upper ocean, *J. Geophys. Res.*, 115, C04026, <https://doi.org/10.1029/2009JC005853>, 2010.
- 995 Huang, C., Qiao, F., Song, Z., and Ezer, T.: Improving simulations of the upper ocean by inclusion of surface waves in the Mellor-Yamada turbulence scheme, *J. Geophys. Res.*, 116, C01007, <https://doi.org/10.1029/2010JC006320>, 2011.
- Janssen, P. E. A. M.: Quasi-linear theory of wind-wave generation applied to wave forecasting, *J. Phys. Oceanogr.* 21, 1631-1642, 1991.
- 1000

- Janssen, P. E. A. M. (Eds.): The interaction of ocean waves and wind, Cambridge University Press, Cambridge, UK, 300pp., ISBN 978-0-521-12104-0, 2004.
- Janssen, P. A. E. M., Giinther, H., Hasselmann, S., Hasselmann, K., Komen, G. J., and Zambresky, L.: Simple tests, in: Dynamics and Modelling of Ocean Waves, edited by: Komen, G. J., Cavaleri, L., Donelan, M., Hasselmann, K., Hasselmann, S., and Janssen, P. A. E. M., Cambridge University Press, Cambridge, UK, 244-257, ISBN 0-521-47047-1, 1994.
- 1005
- Kinsman, B. (Eds.): Wind Waves: Their Generation and Propagation on the Ocean Surface, Dover Publications, Inc., New York, USA, 676 pp., ISBN 978-0-486-64652-7, 2012.
- 1010
- Komen, G. J., Hasselmann, S., and Hasselmann, K.: On the existence of a fully developed windsea spectrum, *J. Phys. Oceanogr.*, 14, 1271-1285, 1984.
- Komen, G. I., Cavaleri, L., Donelan, M., Hasselmann, K., Hasselmann, S., and Janssen, P.A.E.M. (Eds.): Dynamics and Modelling of Ocean Waves. Cambridge University Press, Cambridge, UK, 532pp., ISBN 0-521-47047-1, 1994.
- 1015
- Lamarre, E., and Melville, W. K.: Air entrainment and dissipation in breaking waves, *Nature*, 351, 469-472, 1991.
- Liu, Q., Rogers, W. E., Babanin, A. V., Young, I. R., Romero, L., Zieger, S., Qiao, F., and Guan, C.: Observation-based source terms in the third-generation wave model WAVEWATCH III: Updates and verification, *J. Phys. Oceanogr.*, 49, 489-517, <https://doi.org/10.1175/JPO-D-18-0137.1>, 2019.
- 1020
- Longuet-Higgins, M. S.: The statistical analysis of a random, moving surface, *Philos. Trans. Roy. Soc. London*, 249A, 321-387, 1957.
- Longuet-Higgins, M. S.: On wave breaking and equilibrium spectrum of wind, *Proc. Roy. Soc. London*, 310A, 151-159, 1969.
- 1025
- McWilliams, J. C., Sullivan, P. P., and Moeng, C.-H.: Langmuir turbulence in the ocean. *J. Fluid Mech.*, 334, 1-30, 1997.
- Mellor, G.L., and Yamada, T.: Development of a turbulence closure model for geophysical fluid problems, *Rev. Geophys. Space Phys.*, 20, 851-875, 1982.
- 1030
- Melville, W. K., Loewen, M. R., and Lamarre, E.: Sound production and air

entrainment by breaking waves: A review of recent laboratory experiments, in: *Breaking Waves: IUTAM Symposium, Sydney, Australia, 1991*, edited by: Banner, M. L. and Grimshaw, R. H. J., Springer-Verlag, Berlin, Heidelberg, 139-146, ISBN 978-3-540-55944-3, 1992.

1035 Phillips, O. M.: Spectral and statistical properties of the equilibrium range in wind-generated gravity waves, *J. Fluid Mech.*, 156, 505-531, 1985.

Polnikov, V. G.: On a description of a wind-wave energy dissipation function, in: *The Air-Sea Interface: Radio and Acoustic Sensing, Turbulence and Wave Dynamics*, edited by: Donelan, M. A., Hui, W. H., and Plant, W. J., RSMAS/University of
1040 Miami, 277-282, ISBN 0-930050-00-2, 1994.

Polnikov, V. G.: Wind-wave model with an optimized source function (English transl.), *Izv., Atmos. Ocean. Phys.*, 41(5), 594-610, 2005.

Polnikov, V. G.: An extended verification technique for solving problems of numerical modeling of wind waves (English transl.), *Izv., Atmos. Ocean. Phys.*, 46(4), 511-
1045 523, 2010.

Polnikov, V.G.: Spectral description of the dissipation mechanism for wind waves. Eddy viscosity model, *Mar. Sci.*, 2(3), 13-26.
<https://doi.org/10.5923/j.ms.20120203.01>, 2012

Polnikov, V. G., and Tkalich, P.: Influence of the wind waves dissipation processes on
1050 dynamics in the water upper layer, *Ocean Modell.*, 11, 193-213,
<https://doi.org/10.1016/j.ocemod.2004.12.006>, 2006.

Qiao, F., Yuan, Y., Ezer, T., Xia, C., Yang, Y., Lv, X., and Song, Z.: A three-dimensional surface wave–ocean circulation coupled model and its initial testing, *Ocean Dyn.*, 60(5), 1339-1355, <https://doi.org/10.1007/s10236-010-0326-y>, 2010.

1055 Qiao, F., Yuan, Y., Yang, Y., Zheng, Q., Xia, C., and Ma, J.: Wave-induced mixing in the upper ocean: Distribution and application to a global ocean circulation model, *Geophys. Res. Lett.*, 31, L11303, <https://doi.org/10.1029/2004GL019824>, 2004.

Rogers, W. E., Babanin, A. V., and Wang, D. W.: Observation consistent input and whitecapping dissipation in a model for wind-generated surface waves:
1060 Description and simple calculations, *J. Atmos. Ocean. Technol.*, 29, 1329-1346,
<https://doi.org/10.1175/JTECH-D-11-00092.1>, 2012.

- Shi, Y., Wu, K., and Yang, Y.: Preliminary results of assessing the mixing of wave transport flux residual in the upper ocean with ROMS, *J. Ocean Univ. China*, 15(2), 193-200, <https://doi.org/10.1007/s11802-016-2706-5>, 2016.
- 1065 Shi, Y., Yang, Y., Qi, J., and Wang, H.: Adaptability assessment of the whitecap statistical physics model with cruise observations under high sea states, *Front. Mar. Sci.* 12:1486860, <https://doi.org/10.3389/fmars.2025.1486860>, 2025.
- Shi, Y., Yang, Y., Teng, Y., Sun, M., and Yun, S.: Analysis on the formation of sea ice based on comprehensive observation data, *J. Oceanol. Limnol.*, 37(6), 1846-1856, 1070 <https://doi.org/10.1007/s00343-019-8269-8>, 2019.
- Shu, Q., Qiao, F., Song, Z., Xia, C., and Yang, Y.: Improvement of MOM4 by including surface wave-induced vertical mixing, *Ocean Modell.*, 40, 42-51, <https://doi.org/10.1016/j.ocemod.2011.07.005>, 2011.
- Sun, M., Yang, Y., Shi, Y., and Teng, Y.: Data and comparison results, Zenodo [data set], <https://doi.org/10.5281/zenodo.19230125>, 2026. 1075
- Teixeira, M. A. C., and Belcher, S. E.: On the distortion of turbulence by a progressive surface wave, *J. Fluid Mech.*, 458, 229-267, 2002.
- The WAVEWATCH III® Development Group (WW3DG): User manual and system documentation of WAVEWATCH III® version 6.07, Tech. Note 333, 1080 NOAA/NWS/NCEP/MMAB, College Park, MD, USA, 465 pp. +Appendices, 2019.
- Tolman, H. L.: A third-generation model for wind waves on slowly varying, unsteady and inhomogeneous depths and currents, *J. Phys. Oceanogr.*, 21, 782-797, 1991.
- Tolman, H. L.: Effects of numerics on the physics in a third-generation wind-wave 1085 model, *J. Phys. Oceanogr.*, 22, 1,095-1,111, 1992.
- Tolman, H. L.: Validation of WAVEWATCH III version 1.15 for a global domain, Tech. Note 213, NOAA/NWS/NCEP/OMB, 33 pp., 2002.
- Tolman, H. L., and Chalikov, D.: Source terms in a third-generation wind-wave model, *J. Phys. Oceanogr.*, 26, 2497-2518, 1996.
- 1090 Wang, F., Yang, Y., Yin, X., Jiang, X., and Sun, M.: Improving wave modeling performance by incorporating wave-generated turbulence dissipation and

improved post-breaking spectrum, *Ocean Modell.*, 188 (2024) 102311,
<https://doi.org/10.1016/j.ocemod.2023.102311>, 2024.

1095 Wang, H., Yang, Y., Sun, B., and Shi, Y.: Improvements to the statistical theoretical
model for wave breaking based on the ratio of breaking wave kinetic and potential
energy, *Sci. China Earth Sci.*, 60(1), 180-187, <https://doi.org/10.1007/s11430-016-0053-3>, 2017.

1100 Wang, H., Yang, Y., Dong, C., Su, T., Sun, B., and Zou, B.: Validation of an improved
statistical theory for sea surface whitecap coverage using satellite remote sensing
data, *Sensors*, 18, 3306, <https://doi.org/10.3390/s18103306>, 2018.

WAMDI Group: The WAM model-A third generation ocean wave prediction model, *J.
Phys. Oceanogr.*, 18, 1775-1810, 1988.

1105 Wei, L., Guan, C., and Troitskaya, Y.: Laboratory experiment on wave induced
turbulence, *J. Ocean Univ. China*, 17 (4), 721-726,
<https://doi.org/10.1007/s11802-018-3528-4>, 2018.

Xia, C., Qiao, F., Zhang, M., Yang, Y., and Yuan, Y.: Simulation of double cold cores
of the 35°N section in the Yellow Sea with a wave-tide-circulation coupled model,
Chin. J. Oceanol. Limnol., 22(3), 292-298, 2004.

1110 Xia, C., Qiao, F., Yang, Y., Ma, J., and Yuan, Y.: Three-dimensional structure of the
summertime circulation in the Yellow Sea from a wave-tide-circulation coupled
model, *J. Geophys. Res.*, 111, C11S03, <https://doi.org/10.1029/2005JC003218>,
2006.

Xu, D., and Yu, D. (Eds.): *Theory of random ocean waves*, Higher Education Press,
Beijing, China, 390pp., ISBN 7-04-009922-5, 2001.

1115 Yang, Y., Qiao, F., Xia, C., Ma, J., and Yuan, Y.: Effect of ocean wave momentum and
mixing on upper ocean (in Chinese), *Adv. Mar. Sci.*, 21(4), 363-368, 2003.

Yang, Y., Qiao, F., Xia, C., Ma, J., and Yuan, Y.: Wave-induced Mixing in the Yellow
Sea, *Chin. J. Oceanol. Limnol.*, 22(3), 322-326, 2004.

1120 Yang, Y., Qiao, F., Zhao, W., Teng, Y., and Yuan, Y.: MASNUM ocean wave model in
spherical coordinate and its application, *Acta Oceanol. Sin.*, 27(2), 1-7, 2005.

Yang, Y., Shi, Y., Yu, C., Teng, Y., and Sun, M.: Study on surface wave-induced

- mixing of transport flux residue under typhoon conditions, *J. Oceanol. Limnol.*, 37(6), 1837-1845, <https://doi.org/10.1007/s00343-019-8268-9>, 2019.
- 1125 Yang, Y., Sun, M., Sun, L., Xia, C., Teng, Y., and Cui, X.: A Characteristics Set Computation Model for Internal Wavenumber Spectra and Its Validation with MODIS Retrieved Parameters in the Sulu Sea and Celebes Sea, *Remote Sens.*, 14, 1967, <https://doi.org/10.3390/rs14091967>, 2022.
- Yang, Y., Sun, M., Jiang, X., and Yin, X.: The MASNUM wave model, Zenodo [code], <https://doi.org/10.5281/zenodo.19229991>, 2026.
- 1130 Yefimov, V. V., and Khristoforov, G. N.: Spectra and statistical relations between the velocity fluctuations in the upper layer of the sea and surface waves, *Izv. Acad. Sci. USSR Atmos. Oceanic Phys., Engl. Transl.*, 7, 1290-1310, 1971.
- Young, I. R., and Babanin, A. V.: Spectral distribution of energy dissipation of wind-generated waves due to dominant wave breaking, *J. Phys. Oceanogr.*, 36, 376-394, 1135 <https://doi.org/10.1175/JPO2859.1>, 2006.
- Young, I. R., Babanin, A. V., and Zieger, S.: The decay rate of ocean swell observed by altimeter, *J. Phys. Oceanogr.*, 43, 2322-2333, <https://doi.org/10.1175/JPO-D-13-083.1>, 2013.
- 1140 Yu, C., Yang, Y., Yin, X., Sun, M., and Shi, Y.: Impact of Enhanced Wave-Induced Mixing on the Ocean Upper Mixed Layer during Typhoon Nepartak in a Regional Model of the Northwest Pacific Ocean, *Remote Sens.*, 12, 2808, <https://doi.org/10.3390/rs12172808>, 2020.
- 1145 Yuan, Y. (Eds.): The governing equation sets of the ocean dynamic system and their analytical application examples (in Chinese), Science Press, Beijing, China, 415pp., ISBN 978-7-03-074846-1, 2024.
- Yuan, Y., Tung, C. C., and Huang, N. E.: Statistical characteristics of breaking waves, in: *Wave Dynamics and Radio Probing of the Ocean Surface*, edited by: Phillips, O. M., and Hasselmann, K., Plenum Press, New York, 265-272, ISBN 0-306-41992-0, 1986.
- 1150 Yuan, Y., Hua, F., Pan, Z., and Sun, L.: LAGFD-WAM numerical wave model-I. Basic physical model, *Acta Oceanol. Sin.*, 10(4), 483-488, 1991.
- Yuan, Y., Hua, F., Pan, Z., and Sun, L.: Dissipation source function and improvement

- of LAGFD-WAM numerical wave model, *Oceanol. Limnol. Sin.*, 24(4), 367-376, 1993.
- 1155 Yuan, Y., Han, L., Hua, F., Zhang, S., Qiao, F., Yang, Y., and Xia, C.: The statistical theory of breaking entrainment depth and surface whitecap coverage of real sea waves, *J. Phys. Oceanogr.*, 39, 143-161, <https://doi.org/10.1175/2008JPO3944.1>, 2009.
- 1160 Yuan, Y., Qiao, F., Hua, F., and Wang, Z.: The development of a coastal circulation numerical model: I. Wave-induced mixing and wave-current interaction, *J. Hydrodyn. Ser. A*, 14, 1-8, 1999.
- Yuan, Y., Qiao, F., Yin, X., and Han, L.: Establishment of the ocean dynamic system with four sub-systems and the derivation of their governing equation sets, *J. Hydrodyn.*, 24, 153-168, [https://doi.org/10.1016/S1001-6058\(11\)60231-X](https://doi.org/10.1016/S1001-6058(11)60231-X), 2012.
- 1165 Yuan, Y., Qiao, F., Yin, X., and Han, L.: Analytical estimation of mixing coefficient induced by surface wave-generated turbulence based on the equilibrium solution of the second-order turbulence closure model, *Sci. China Earth Sci.*, 56, 71-80, <https://doi.org/10.1007/s11430-012-4517-x>, 2013.
- 1170 Zieger, S., Babanin, A. V., Rogers, W. E., and Young, I. R.: Observation-based source terms in the third-generation wave model WAVEWATCH, *Ocean Modell.*, 96, 2-25, <https://doi.org/10.1016/j.ocemod.2015.07.014>, 2015.
- Zhuang, Z., Zheng, Q., Yuan, Y., Yang, G., and Zhao, X.: A non-breaking-wave-generated turbulence mixing scheme for a global ocean general circulation model, *Ocean Dyn.*, 70, 293-305, <https://doi.org/10.1007/s10236-019-01338-3>, 2020.
- 1175 Zhuang, Z., Zheng, Q., Yang, Y., Song, Z., Yuan, Y., Zhou, C., Zhao, X., Zhang, T., and Xie, J.: Improved upper-ocean thermodynamical structure modeling with combined effects of surface waves and M_2 internal tides on vertical mixing: a case study for the Indian Ocean, *Geosci. Model Dev.*, 15, 7221-7241, <https://doi.org/10.5194/gmd-15-7221-2022>, 2022.
- 1180 Zhuang, Z., Yuan, Y., Zheng, Q., Zhou, C., Zhao, X., and Zhang, T.: Effects of buoyancy flux on upper-ocean turbulent mixing generated by nonbreaking surface waves observed in the South China Sea, *J. Geophys. Res.*, 126, e2020JC016816, <https://doi.org/10.1029/2020JC016816>, 2021.

